

1 **Biogeochemical processes captured by carbon isotopes in**
2 **redox-stratified water columns: a comparative study of four**
3 **modern stratified lakes along an alkalinity gradient.**

4

5 Robin Havas^{a,*}, Christophe Thomazo^{a,b}, Miguel Iniesto^c, Didier Jézéquel^d, David Moreira^c, Rosaluz Tavera^c,
6 Jeanne Caumartin^f, Elodie Muller^f, Purificación López-García^c, Karim Benzerara^f

7

8 ^a Biogéosciences, CNRS, Université de Bourgogne Franche-Comté, 21000 Dijon, France

9 ^b Institut Universitaire de France, 75005 Paris, France

10 ^c Ecologie Systématique Evolution, CNRS, Université Paris-Saclay, AgroParisTech, 91190 Gif-sur-Yvette,
11 France

12 ^d IPGP, CNRS, Université de Paris, 75005 Paris, and UMR CARRTEL, INRAE & USMB, France

13 ^e Departamento de Ecología y Recursos Naturales, Universidad Nacional Autónoma de México, México

14 ^f Sorbonne Université, Muséum National d'Histoire Naturelle, CNRS, Institut de Minéralogie, de Physique des
15 Matériaux et de Cosmochimie (IMPMC), 75005 Paris, France.

16

17

18 * Correspondence to: Robin Havas (robin.havas@gmail.com)

Field Code Changed

19

20

21

22

23

24

Keywords: Carbon cycle; DIC; POC; isotopic fractionation; Precambrian analogues

25 **Abstract.** Redox-stratified water columns are a prevalent feature of Earth history, and ongoing environmental
 26 changes tend to promote a resurgence of such settings. Studying modern redox-stratified environments has
 27 improved our understanding of biogeochemical processes and element cycling in such water columns. These
 28 settings are associated with peculiar carbon biogeochemical cycling owing to a layered distribution of biological
 29 processes in relation to oxidant availability. Metabolisms from distinct biogeochemical layers are diverse and may
 30 differently imprint the sedimentological record. Paired carbon isotope compositions of organic matter and
 31 carbonates, which are commonly used to characterize these ecological dynamics, can thus vary from one stratified
 32 environment to another. Changes in the organic/inorganic carbon sources and mass balance can further complicate
 33 the isotopic message in stratified environments. Better understanding of these multifaceted carbon isotope signals
 34 requires further evaluation of how the processes occurring in redox-stratified water columns are transferred to the
 35 sediments. We therefore characterized and compared the isotopic signatures of dissolved inorganic carbon (DIC),
 36 carbonate, and organic matter reservoirs, at different depths in the water column and upper sediments of four
 37 stratified Mexican lakes that follow a gradient of alkalinity/salinity. Comparing these systems shows strong
 38 diversity in the carbon isotope signals of the water column and sediments. Differences in inorganic carbon isotope
 39 signatures arise primarily from the size of the DIC reservoir, buffering the expression of redox-dependent
 40 biological processes as alkalinity increases. Combining this isotopic dataset with water-column physico-chemical
 41 parameters allows us to identify oxygenic photosynthesis and aerobic respiration in the four lakes studied, while
 42 anoxygenic photosynthesis is evidenced in only two of them. Sedimentary organic matter does not originate from
 43 the same water-column layers in the four lakes, highlighting the ecological variability that can stem from different
 44 stratified water columns, and how it is transferred or not to the sedimentary record. The least alkaline lake shows
 45 higher isotopic variability, and signatures typical of methanogenesis in the sediment porewaters. This metabolism,
 46 however, does not leave diagnostic isotopic signatures in the sedimentary archives (organic matter and carbonates),
 47 underlining the fact that even when alkalinity does not strongly buffer the inorganic carbon reservoir, a
 48 comprehensive picture of the active biogeochemical carbon cycling is not necessarily transferred to the geological
 49 record.

50

- Deleted: different
- Deleted: These processes and their sedimentological expression, notably inferred from
- Deleted: p
- Deleted: –
- Deleted:
- Deleted: isotopic compositions of carbon,
- Deleted: , because metabolisms from different biogeochemical layers are diverse and may differently imprint the sedimentological record
- Deleted: This variability can arise from numerous physico-chemical parameters, such as sedimentation rate, pH, trace element availability, or basin physiography.
- Deleted: these
- Deleted: systems
- Deleted: the transfer function from the processes occurring in redox-stratified water columns to
- Deleted:
- Deleted: organic matter,
- Deleted: dissolved inorganic carbon (DIC)
- Deleted: both
- Deleted: ary carbon isotope signals
- Deleted: s
- Deleted: of the water columns
- Deleted: the activity of
- Deleted: However,
- Deleted: s
- Deleted:
- Deleted: distinct
- Deleted: it
- Deleted: is

82 1. INTRODUCTION

83 The carbon cycle and biogeochemical conditions prevailing at the surface of the Earth are intimately bound through
84 biological (e.g. photosynthesis) and geological processes (e.g. volcanic degassing and silicate weathering). The
85 analysis of carbon isotopes in organic matter and carbonates ($\delta^{13}\text{C}_{\text{org}}$ and $\delta^{13}\text{C}_{\text{carb}}$) in the rock record, has been used
86 to reconstruct the evolution of the biosphere and the oxygenation of the Earth's surface (e.g. Hayes et al., 1989;
87 Karhu and Holland, 1996; Schidlowski, 2001). Coupling $\delta^{13}\text{C}_{\text{org}}-\delta^{13}\text{C}_{\text{carb}}$ has frequently been used to infer the burial
88 rate of organic C, and thus the redox balance of the atmosphere and hydrosphere (e.g. Karhu and Holland, 1996;
89 Aharon, 2005; Krissansen-Totton et al., 2015; Mason et al., 2017). It has also been used to deduce the presence of
90 metabolisms like anoxygenic chemoautotrophic or methanotrophic bacteria (e.g. Hayes et al., 1999; Bekker et al.,
91 2008; Krissansen-Totton et al., 2015). Coupling $\delta^{13}\text{C}_{\text{org}}-\delta^{13}\text{C}_{\text{carb}}$ has also been used to discuss oceans stratification
92 and its effect on inorganic and organic C geochemical signatures in sediments (e.g. Logan et al., 1995; Aharon,
93 2005; Bekker et al., 2008; Ader et al., 2009). Stratification favors the expression and recording of different layers
94 of the water column, with potentially very distinct isotopic signatures. As the oceans were redox-stratified during
95 most of the Earth's history (Lyons et al., 2014; Havig et al., 2015; Satkoski et al., 2015), processes affecting the C
96 cycle were likely different from those occurring in most modern, well-oxygenated environments. This change of
97 conditions could impact the $\delta^{13}\text{C}_{\text{org}}$ signal at various scales, from changes in diversity and relative abundance of
98 microbial carbon and energy metabolism (e.g. Wang et al., 2016; Iniguez et al., 2020; Hurley et al., 2021), to larger
99 ecological interactions (e.g. Jiao et al., 2010; Close and Henderson, 2020; Klawonn et al., 2021) and global C
100 dynamics (e.g. Ridgwell and Arndt, 2015; Ussiri and Lal, 2017).

101 Modern stratified lakes have been used as analogues of ancient redox-stratified systems to better understand the C
102 cycle in the sedimentary isotopic record (e.g. Lehmann et al., 2004; Posth et al., 2017; Fulton et al., 2018). Several
103 number of recent studies have investigated the C cycle in modern stratified water columns (e.g. Crowe et al., 2011;
104 Kuntz et al., 2015; Posth et al., 2017; Schiff et al., 2017; Havig et al., 2018; Cadeau et al., 2020; Saini et al., 2021;
105 Petrash et al., 2022), where many bio-geo-physico-chemical parameters can be directly measured, together with
106 the main C reservoirs. However, investigations of such Precambrian analogues do not necessarily include sediment
107 data, and generally focus on a single environment without integrating views from several systems.

108 In this study, we measured the concentrations and isotopic compositions of dissolved inorganic carbon (DIC) and
109 particulate organic carbon (POC) throughout the water column of four modern redox-stratified alkaline crater
110 lakes, located in the Trans-Mexican Volcanic Belt (Ferrari et al., 2012). We also measured the concentrations and
111 isotopic compositions of the sedimentary organic carbon and carbonates as well as porewater DIC from surficial
112 sediments (~ 10 cm) at the bottom of the lakes. The four lakes share similar geological and climatic contexts but
113 have distinct solution chemistries along a marked alkalinity–salinity gradient (Zeyen et al., 2021) – as well as
114 distinct planktonic communities (Iniesto et al., 2022). We therefore seek to evaluate how these environmental and
115 ecological differences are recorded in the C isotope signatures in the water columns (DIC–POC) and sedimentary
116 archives (organic matter–carbonates). The four lakes are closed lakes in endorheic basins (Alcocer, 2021; Zeyen
117 et al., 2021), which facilitates the identification of external environmental constraints (e.g. evaporation, C sources)
118 and their influence on processes occurring within the water columns. Depth profiles of the main physico-chemical
119 parameters together with trace and major elements concentrations were measured to pinpoint the dominant
120 biogeochemical processes occurring in the water columns and link them to specific C isotopes signatures.

121 First, we constrain the main DIC sources and external controls on the lakes' alkalinity. Next, we describe the
122 influence of the inter-lake alkalinity gradient on the inorganic C cycle and stratification of the lakes, and how it is
123 recorded in surficial sediments. Then, by combining POC and DIC data, we identify the sources of organic C to
124 the lakes by describing the main autotrophic reactions occurring in the water columns (e.g. oxygenic and
125 anoxygenic photosynthesis). Finally, we discuss the fate of POC, either recycled (e.g. via methanogenesis) or
126 deposited in the sediments, and how all these processes are recorded (or not) in surficial sediments.

127

128 2. SETTING / CONTEXT

129 2.1. Geology

130 The four lakes studied here are volcanic maars formed after phreatic, magmatic, and phreatomagmatic explosions,
131 related to volcanic activity in the Trans-Mexican Volcanic Belt (TMVB, Fig. 1). The TMVB originates from the
132 subduction of the Rivera and Cocos plates beneath the North America plate, resulting in a long (~1000 km) and
133 wide (90–230 km) Neogene volcanic arc spreading across central Mexico (Ferrari et al., 2012). The TMVB harbors
134 a large variety of monogenetic scoria cones and phreatomagmatic vents (maars and tuff-cones) as well as
135 stratovolcanoes, calderas, and domes (Carrasco-Núñez et al., 2007; Ferrari et al., 2012; Siebe et al., 2014). Maar
136 crater formation usually occurs when ascending magma meets water-saturated substrates, leading to successive
137 explosions and the excavation of older units (Lorenz, 1986; Carrasco-Núñez et al., 2007; Siebe et al., 2012; Chako
138 Tchamabé et al., 2020).

139 The first lake, La Alberca de los Espinos (1985 masl), is located at the margin of the Zacapu tectonic lacustrine
140 basin in the Michoacán-Guanajuato Volcanic Field (MGVF) in the central-western part of the TMVB (Fig. 1). It
141 lies on andesitic basement rocks and was dated at -25 ± 2 ka (Siebe et al., 2012, 2014). The other three lakes (La
142 Preciosa, Atexcac and Alchichica) are all in the same area (~ 50 km²) of the Serdan-Oriental Basin (SOB) in the
143 easternmost part of the TMVB (Fig. 1). The SOB is a closed intra-montane basin at high altitude (~2300 m),
144 surrounded by the Los Humeros caldera to the north and the Cofre de Perote-Citlatépel volcanic range to the east.
145 The basement is composed of folded and faulted Cretaceous limestones and shales, covered by andesitic-to-basaltic
146 lava flows (Carrasco-Núñez et al., 2007; Armienta et al., 2008; Chako Tchamabé et al., 2020). The Alchichica and
147 Atexcac craters was dated at $\sim 6-13 \pm 5-6$ ka (Chako Tchamabé et al., 2020) and 330 ± 80 ka (Carrasco-Núñez et
148 al., 2007), respectively (Table 1). The age of La Preciosa is not known.

149

150 2.2. Climate and limnology

151 La Alberca is a freshwater lake (0.6 psu) with a temperate to semi-humid climate (Rendon-Lopez, 2008; Sigala et
152 al., 2017). In contrast, lakes from the SOB experience a similar temperate to semi-arid climate (Armienta et al.,
153 2008; Sigala et al., 2017). The current climate of the SOB is dominated by dry conditions, reflected by higher
154 evaporation than precipitation fluxes in Lake Alchichica (~ 1686 vs. 392 mm/year; Alcocer, 2021). In La Preciosa,
155 Atexcac, and Alchichica, **significant evaporation** is reflected by a drop in water level, evidenced by the emersion
156 of microbialite deposits (Fig. S1; Zeyen et al., 2021). This evaporation-dominated climate strongly contributes to
157 the relatively high salinity values in these lakes (1.2–7.9 psu), ranging from sub- to hyposaline.

Deleted: this trend

159 The four lakes are warm monomictic: they are stratified for about nine months of the year, mixing only when
160 thermal stratification breaks down in the cold of winter (Armienta et al., 2008). They are all closed lakes located
161 in an “endorheic” basin (Alcocer, 2021; Zeyen et al., 2021), meaning that they have no inflow, outflow, or
162 connection to other basins through surficial waters such as streams. The only water input is from precipitation and
163 groundwater inflow (quantified for Lake Alchichica; Alcocer, 2021 and references therein).

164 The four lakes are alkaline (pH ~ 9) but cover a broad range of chemical compositions (including alkalinity,
165 salinity, and Mg/Ca ratio), interpreted as reflecting different concentration stages of an initial alkaline dilute water
166 (Table 1; Zeyen et al., 2021). Variations in concentration stages may be due to differences in climate and, more
167 generally, different hydrological regimes. Microbialite deposits are found in all four lakes (Gérard et al., 2013;
168 Saghaï et al., 2016; Iniesto et al., 2021a, 2021b; Zeyen et al., 2021), and increase in abundance from lower to
169 higher alkalinity conditions (Zeyen et al., 2021).

170

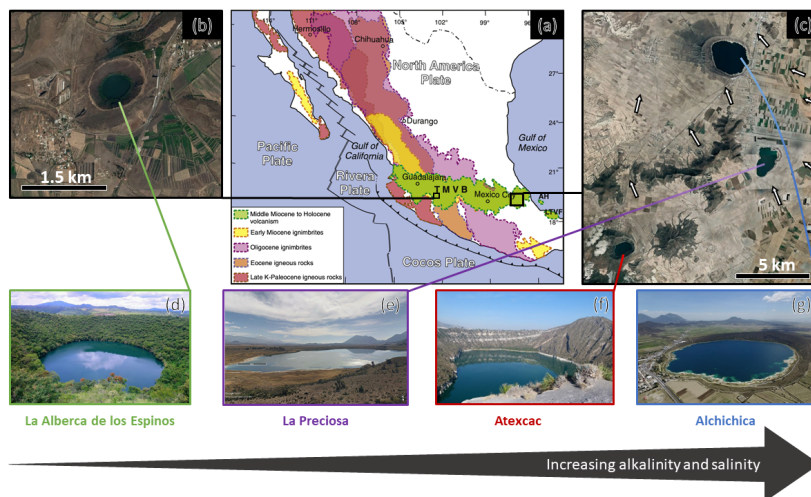
171 3. METHOD

172 3.1. Sample Collection

173 The sediment core from Lake La Preciosa was collected in May 2016. All other samples were collected in May
174 2019. The depth profiles of several physico-chemical parameters were measured in the water columns of the four
175 lakes using an YSI Exo 2 multi-parameter probe: temperature, pH, ORP (oxidation reduction potential),
176 conductivity, O₂, chlorophyll a, phycocyanin, and turbidity. Precisions for these measurements were 0.01 °C, 0.1
177 pH unit, 20 mV, 0.001 mS/cm, 0.1 mg/L, 0.01 µg/L, 0.01 µg/L and 2% FTU unit, respectively. The ORP signal
178 was not calibrated before each profile and is thus used to discuss relative variations over a depth profile.
179 Measurements of the aforementioned parameters served to pinpoint depths of interest for further chemical and
180 isotopic analyses, notably around the redoxcline of the lakes. Water samples were collected with a Niskin bottle.
181 Particulate matter was collected on pre-combusted (2 h at 490°C) and weighted glass fiber filters (Whatman GF/F,
182 0.7 µm) and analyzed for particulate organic carbon (POC), major and trace elements. Between 1.5 and 5 L of lake
183 water was filtered before the GF/F filters became clogged. The processed solution was filtered again at 0.22 µm
184 with Filtropur S filters (pre-rinsed with lake water filtered at 0.7 µm) for analyses of dissolved inorganic carbon
185 (DIC), and major, minor, and trace ions.

186 Sediment cores were collected using a 90 mm Uwitec corer close to the deepest point of each lake’s water column
187 (Table 1), where anoxic conditions prevail almost all year long. Cores measured between 20 and 85 cm in length.
188 Slices of about 2-3 cm were cut under anoxic conditions, using a glove bag filled with N₂ (anoxia was monitored
189 using a WTW3630 equipped with a FDO O₂ optode). Interstitial porewater was drained out of the core slices using
190 Rhizons in the glove bag. Sediments were transported back to the laboratory within aluminized foils (Protpack,
191 UK). Sediments were then fully dried in a laboratory anoxic N₂-filled glove box.

192



193 Figure 1. Geographical location and photographs of the four crater lakes. (a) Geological map from Ferrari et al.
 194 (2012) with black squares showing the location of the four studied lakes within the Trans-Mexican Volcanic Belt
 195 (TMVB). (b, c) Close up © Google Earth views of La Alberca de los Espinos and the Serdan-Oriental Basin
 196 (SOB). The white arrows represent the approximate groundwater flow path (based on Silva-Aguilera, 2019). (d-
 197 g) Photographs of the four lakes (d from © Google Image [‘enamoredemexicowebsite’], e from © Google Earth
 198 street view, and g from © ‘Agencia Es Imagen’).

199

Lake	General location	Sampling location	Elevation (masl)
Alchichica	Serdan Oriental Basin, eastern TMVB	19°24'51,5" N; 97°24'09,9" W	2320
Atexcac	Serdan Oriental Basin, eastern TMVB	19°20'2.2" N; 97°26'59.3" W	2360
La Preciosa	Serdan Oriental Basin, eastern TMVB	19°22'18.1" N; 97°23'14.4" W	2330
La Alberca de los Espinos	Zacapu Basin, MGVF, central TMVB	19°54'23.9" N; 101°46'07.8" W	1985

200

Lake	Lake Basement	Age	Max Depth (m)	Alkalinity (mmoles/L)	Salinity (psu)	pH
Alchichica	limestone, basalts	6-13 ± 5-6 ka	63	~35	7.9	9.22
Atexcac	limestone, andesites, basalts	330 ± 80 ka	39	~26	7.4	8.85
La Preciosa	limestone, basalts	Pleistocene	46	~13.5	1.15	9.01
La Alberca de los Espinos	andesite xenoliths	25 ± 2 ka	30	~7	0.6	9.14

201

202 Table 1. General information about the lakes studied. Abbreviations: TMVB: Trans-Mexican Volcanic Belt;
 203 MGVF: Michoacán-Guanajuato Volcanic Field; masl.: meters above sea level. NB: Sampling took place in
 204 May 2019, except for La Preciosa sediments, sampled in May 2016.

205 **3.2. Dissolved inorganic carbon (DIC) concentration and isotope measurements**

206 Twelve mL of the 0.7- μm filtered lake water was filtered at 0.22- μm directly into hermetic Exetainer® tubes to
207 avoid exchange between DIC and atmospheric CO_2 . The DIC concentrations and isotopic compositions were
208 measured at the Institut de Physique du Globe de Paris (IPGP, France), using an Analytical Precision 2003 GC-
209 IRMS, running under He-continuous flow, following the protocol described by Assayag et al. (2006). A given
210 volume of the solution was extracted from the Exetainer® tube with a syringe, while the same volume of helium
211 was introduced to maintain stable pressure and atmospheric- CO_2 -free conditions within the sample tubes. The
212 collected sample was inserted into another Exetainer® tube, pre-filled with a few drops of 100% phosphoric acid
213 (H_3PO_4) and pre-flushed with He gas. Under acidic conditions, DIC quantitatively converts to gaseous and aqueous
214 CO_2 , which equilibrates overnight within the He-filled head space of the tube. Quantification and isotopic analyses
215 of released gaseous CO_2 were then carried out by GC-IRMS using internal standards of known composition that
216 were prepared and analyzed via the same protocol. Each measurement represented an average of four injections in
217 the mass spectrometer. Chemical preparation and IRMS analysis were duplicated for all the samples. The $\delta^{13}\text{C}_{\text{DIC}}$
218 reproducibility calculated for the 65 samples was better than ± 0.2 ‰, including internal and external
219 reproducibility. Standard deviation for [DIC] was 0.6 ± 0.9 mmol/L on average.

220 Specific DIC speciation, i.e., $\text{CO}_{2(\text{aq})}$, HCO_3^- and CO_3^{2-} activities, was computed using Phreeqc with the full
221 dissolved chemical composition of each sample as an input. It should be noted that these results are calculated
222 from theoretical chemical equilibria and do not necessarily take into account local kinetic effects, which, for
223 example, could lead to local exhaustion of $\text{CO}_{2(\text{aq})}$ where intense photosynthesis occurs.

224

225 **3.3. Particulate organic carbon and nitrogen (POC / PON)**

226 Particulate organic matter from the lake water columns was collected on GF/F filters, dried at room temperature
227 and ground in a ball mill before and after decarbonation. Decarbonation was performed with 12N HCl vapors in a
228 desiccator for 48 h. Aliquots of dry decarbonated samples (25 - 70 mg) were weighed in tin capsules. The POC
229 and PON contents and $\delta^{13}\text{C}_{\text{POC}}$ were determined at the Laboratoire Biogéosciences (Dijon, France) using a Vario
230 MICRO cube elemental analyzer (Elementar, Hanau, Germany) coupled in continuous flow mode with an
231 IsoPrime IRMS (Isoprime, Manchester, UK). The USGS 40 and IAEA 600 certified materials used for calibration
232 showed reproducibility better than 0.15 ‰ for $\delta^{13}\text{C}$. External reproducibility based on triplicate analyses of
233 samples ($n=23$) was 0.1 ‰ on average for $\delta^{13}\text{C}_{\text{POC}}$ (1SD). External reproducibility for POC and PON
234 concentrations was 0.001 and 0.005 mmol/L on average, respectively (i.e. 3 and 7 % of measured concentrations).

235

236 **3.4. Geochemical characterizations of the sediments**

237 Sedimentary organic carbon (SOC), sedimentary organic nitrogen (SON), and their isotopic compositions were
238 measured on carbonate-free residues of the first 12 cm of the sediment cores, produced after overnight 1N HCl
239 digestion. Plant debris (mainly found in La Alberca and Atexcac) was identified upon initial sediment grinding in
240 an agate mortar and analyzed separately. Aliquots of dried decarbonated samples (~4-70 mg) were weighed in tin
241 capsules. The SOC and SON contents and $\delta^{13}\text{C}$ were determined at the Laboratoire Biogéosciences (Dijon) using

242 a Vario MICRO cube elemental analyzer (Elementar GmbH, Hanau, Germany) coupled in continuous flow mode
243 with an IsoPrime IRMS (Isoprime, Manchester, UK). The USGS 40 and IAEA 600 certified materials used for
244 calibration had a reproducibility better than 0.2 ‰ for $\delta^{13}\text{C}_{\text{SOC}}$. Sample analyses (n=67) were at least duplicated
245 and showed an average external reproducibility of 0.1 ‰ for $\delta^{13}\text{C}$ (1SD). External reproducibility for SOC and
246 SON contents was 0.1 and 0.03 wt. %, respectively.

247 Carbon isotope compositions of sedimentary carbonates were analyzed at the Laboratoire Biogéosciences (Dijon)
248 using a ThermoScientific™ Delta V Plus™ IRMS coupled with a Kiel VI carbonate preparation device. External
249 reproducibility was assessed by multiple measurements of NBS19 standard and was better than ± 0.1 ‰ (2σ).
250 Total carbonate concentration was determined by mass balance after decarbonation for SOC analysis.

251 Mineralogical assemblages of sediments were determined on bulk powders by X-Ray diffraction (XRD) at the
252 Laboratoire Biogéosciences (Dijon). Samples were ground in an agate mortar. Diffractograms were obtained with
253 a Bruker D8 Endeavor diffractometer with CuK α radiation and LynxEye XE-T detector, under 40 kV and 25 mA
254 intensity. Mineral identification was based on COD (“Crystallography Open Database”) and BGMN databases.
255 Mineral abundances were estimated by Rietveld refinement analysis implemented in the Profex software.

256 Solid sulfide concentrations were determined on dry bulk sediments from La Alberca Lake after a wet chemical
257 extraction using a boiling acidic Cr(II)-solution as detailed in Gröger et al. (2009).

258

259 **3.5. Major and trace elements concentrations**

260 Dissolved and particulate matter elemental compositions were measured at the Pôle Spectrométrie Océan
261 (Plouzané, France) by inductively coupled plasma–atomic emission spectroscopy (ICP-AES, Horiba Jobin) for
262 major elements and by high-resolution ICP–mass spectrometry using an Element XR (HR-ICP-MS, Thermo Fisher
263 Scientific) for trace elements. Major element measurement reproducibility based on internal multi-elemental
264 solution was better than 5%. Trace elements were analyzed by a standard-sample bracketing method and calibrated
265 with a multi-elemental solution. Analytical precision for trace elements was generally better than 5%. Dissolved
266 sulfate concentrations were analyzed by ion chromatography at the IPGP (Paris, France) with uncertainty lower
267 than 5%.

268

269 **4. RESULTS**

270

271 **4.1. Lake La Alberca de los Espinos**

272 Stratification of the water column was well defined in La Alberca de los Espinos (Fig. 2). Temperature was higher
273 than in the other lakes (decreasing from ~ 23 °C at the surface to 16.5 °C at depth). Dissolved O₂ was oversaturated
274 at the lake surface (118 %, *i.e.*, 7.9 mg/L), rapidly decreasing to 0 between ~ 5 and 12 m, while the oxidation
275 reduction potential (ORP) only decreased below 17 m depth. The offset between O₂ exhaustion and ORP decrease
276 can be explained by the presence of other oxidant species and/or extended chlorophyll a peaks (supplementary
277 text 1). Conductivity decreased from 1.20 to 1.17 mS/cm at 16 m before increasing to 1.27 mS/cm at 26 m (salinity

278 between 0.58 and 0.64 psu). Chlorophyll a (Chl a) averaged 3.1 $\mu\text{g/L}$, and showed a profile with at least three
279 distinctive peaks, (i) between 6 and 9.5 m, (ii) around 12.5 m and (iii) between 16 and 19 m, all reaching $\sim 4 \mu\text{g/L}$.
280 The turbidity profile showed a pronounced increase from 16 to 19 m. The pH profile showed important variation
281 from 9.15 at the lake surface to 8.75 between 6.5 and 10 m, further decreasing to 7.5 between 16 and 26 m. Based
282 on the temperature profiles, epi-, meta- and hypolimnion layers of Lake La Alberca de los Espinos in May 2019
283 broadly extended from 0-5, 5-12 and 12-30 m, respectively (Fig. 2). The conductivity and pH profiles, however,
284 show that different conditions prevail at the top and bottom of the hypolimnion.

285 Dissolved inorganic carbon (DIC) concentration progressively increased from 6.8 mM at 5 m to 8.7 mM at 26 m.
286 The pCO_2 calculated for surface waters was near equilibrium with atmospheric $\text{pCO}_{2\text{atm}}$, but strongly increased
287 with depth, up to ~ 40 times the $\text{pCO}_{2\text{atm}}$ (Table S2). The $\delta^{13}\text{C}_{\text{DIC}}$ first decreased from about -2.5‰ to -4.1‰
288 between 5 and 10 m, before increasing again up to -2‰ at 25 m. Particulate organic carbon (POC) concentrations
289 reached minimum values of 0.02 mM at 10 m but rose to maximum values in the hypolimnion (0.06 mM). The
290 C:N molar ratio of particulate organic matter (POM) progressively decreased from 8.5 at the surface to less than
291 6.5 in the hypolimnion. The $\delta^{13}\text{C}_{\text{POC}}$ had minimum values at 10 and 17 m (-28.3 and -29‰ , respectively). Above
292 and below these depths, $\delta^{13}\text{C}_{\text{POC}}$ averaged $-26.4 \pm 0.5 \text{‰}$.

293 Dissolved sulfates as measured by chromatography were only detectable at 5 m with a low concentration of 12 μM ,
294 while total dissolved S measured by ICP-AES, showed values in the hypolimnion higher than in the upper layers
295 (~ 10.3 vs. 7.4 μM , Table S4). Dissolved Mn concentrations decreased from 1.5 to 0.5 μM between 5 and 10 m,
296 then increased to 2 μM at 25 m. Aqueous Fe was only detectable at 25 m with a concentration of 0.23 μM
297 (Table S4). In parallel, particulate S concentrations increased with depth, with a marked increase from 0.1 to
298 0.6 μM between 20 and 25m. Increase in particulate S was correlated with a 25-fold increase in particulate Fe
299 (from 0.2 to 5.97 μM). Particulate Mn showed a peak between 17 and 20 m around 1 μM , contrasting with values
300 lower than 0.15 μM in the rest of the water column (Fig. 2, Table S5).

301 In the first centimeters of sediments, DIC concentration in the porewater varied between ~ 11 and 12 mM and
302 $\delta^{13}\text{C}_{\text{DIC}}$ varied between $+8$ and $+10 \text{‰}$ (Figs. 3, 4). Surficial sedimentary carbonates corresponded to calcite and
303 had a $\delta^{13}\text{C}$ around -1.5‰ . Sedimentary organic matter had a $\delta^{13}\text{C}_{\text{SOC}}$ increasing from ~ -29.4 to -25.5‰ and a
304 C:N molar ratio varying between 11.6 and 14.3 (Figs. 3, 4; Table S3).

305

306 4.2. Lake La Preciosa

307 Lake La Preciosa was also stratified at the time of sample collection (Fig. 2). Temperature decreased from $\sim 20 \text{ }^\circ\text{C}$
308 at the surface to 16 $^\circ\text{C}$ at 15m depth. Conductivity showed the same trend with values between 2.24 and
309 2.22 mS/cm (salinity around 1.15 psu). Dissolved O_2 was oversaturated at the lake surface (120 %, i.e., 8.4 mg/L),
310 rapidly decreasing to 0 between ~ 8 and 14 m, while the ORP decreased right below 16 m. Chl a concentration
311 averaged 3 $\mu\text{g/L}$ and recorded the highest peak compared to the other lakes (about 9 $\mu\text{g/L}$ at 10 m) before
312 decreasing to 0.7 $\mu\text{g/L}$ below 15 m. Turbidity showed a large peak between 16 and 19 m. The pH showed a small
313 decrease from 9 to 8.8 between the surface and 15 m depth. Based on the temperature profiles, epi-, meta- and
314 hypolimnion layers of La Preciosa in May 2019 broadly extended from 0-6, 6-15 and 15-46 m, respectively
315 (Fig. 2).

Deleted: This

Deleted: spatially

318 The DIC concentration was constant throughout the water column at 13.3 mM, with an exception at 12.5 m, where
 319 it decreased to 11.5 mM (Fig. 3, Table S1). Calculated pCO₂ at the surface represented about two times the
 320 atmospheric pCO_{2atm} (Table S2). The δ¹³C_{DIC} decreased from about 0.5 ‰ to -0.36 ‰ between the surface and the
 321 hypolimnion. The POC concentration decreased from ~0.06 mM in the epi-/metalimnion to 0.02 mM in the
 322 hypolimnion. Similarly, (C:N)_{POM} decreased from ~11.2 in the epi-/metalimnion to 7.6 in the hypolimnion. The
 323 δ¹³C_{POC} increased downward from ~-27 to -25 ‰ to with a peak to -23.5 ‰ at 15 m.

324 In the first 10 cm of sediments, δ¹³C_{SOC} values increased downwards from ~-25.5 to -23.2 ‰ and C:N molar ratio
 325 from 9.8 to 11 (Figs. 3, 4; Table S3). Carbonates corresponded to aragonite and calcite and had a bulk C isotope
 326 composition averaging 2.6 ‰ (Table S3). Porewaters from the 2016 La Preciosa core were not retrieved.

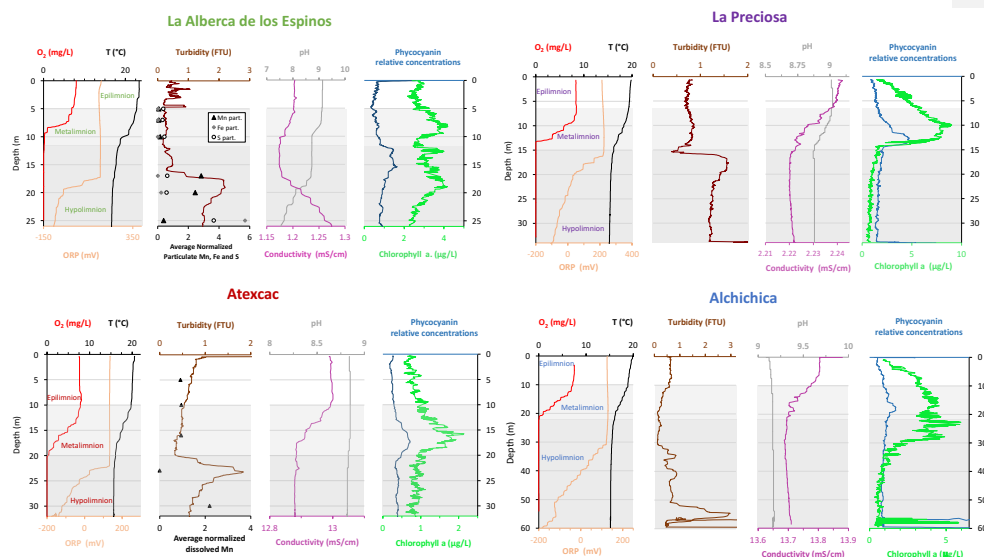


Figure 2. Physico-chemical parameters depth profiles in La Alberca de los Espinos, La Preciosa, Atexcac and Alchichica in May 2019 including: dissolved oxygen concentration (mg/L), water temperature (°C), oxidation-reduction potential (ORP, mV), turbidity (Formazin Turbidity Unit), pH, conductivity (mS/cm), phycocyanin and chlorophyll a pigments (µg/L). Absolute values for phycocyanin concentrations were not determined; only relative variations are represented (with increasing concentrations to the right). Discrete concentration values of dissolved Mn in Atexcac and particulate Mn, Fe and S in La Alberca, normalized by their respective average are represented. Epi-, meta- and hypo-limnion layers are depicted for each lake according to temperature profiles. The three layers closely corresponded to oxygen-rich, oxygen-poor and intermediate zones (except in La Preciosa where the oxycline was slightly thinner than the thermocline layer, ~5 vs. 8 m).

327

328 4.3. Lake Atexcac

329 Stratification of the Lake Atexcac water column was also very well defined (Fig. 2). Temperature decreased from
 330 ~20.6 °C at the surface to reach 16 °C below 20 m. Conductivity showed the same trend with values between 13
 331 and 12.8 mS/cm near the surface (salinity around 7.4 psu). Dissolved O₂ was slightly oversaturated at the lake

332 surface (115 % or 7.6 mg/L), rapidly decreasing to 0 mg/L between ~ 10 and 20 m, while ORP signal decreased
333 below a depth of 22 m. Chl a averaged 1 µg/L and showed a narrow peak centered at around 16 m, reaching
334 ~2 µg/L. Turbidity showed a pronounced increase below 20 m, peaking at 23.3 m and returning to surface values
335 at 26 m. The pH remained around 8.85 throughout the water column. Based on the temperature profiles, the epi-,
336 meta- and hypolimnion of Atexcac in May 2019 broadly extended from 0-10, 10-20 and 20-39 m, respectively
337 (Fig. 2).

338 The DIC concentration was around 26 mM throughout the water column, except at 23 m where it decreased to
339 24.2 mM (Fig. 3, Table S1). Calculated pCO₂ was about five times higher than the atmospheric pCO_{2atm} (Table S2).
340 The δ¹³C_{DIC} was stable around 0.4 ‰ in the epi-/metalimnion, but increased to 0.9 ‰ at 23 m and reached 0.2 ‰
341 minimum values at the bottom of the lake. The POC concentration was ~ 0.05 mM in the epi-/metalimnion,
342 decreasing to 0.02 mM in the hypolimnion. The C:N molar ratio of POM showed the same depth profile, decreasing
343 from ~9.6 in the epi-/metalimnion to 6.6 in the hypolimnion (Fig. 3). The δ¹³C_{POC} showed minimum values in the
344 epi-/metalimnion (-29.3 ‰ at 16 m) and increased to -26.5 ‰ in the hypolimnion.

345 Dissolved sulfate concentration was relatively stable at ~ 2.51 mM throughout the water column but increased to
346 2.64 mM at 23 m. Dissolved Mn concentration was constant at 1 µM down to 16 m before dropping to 0 at 23 m,
347 and increasing again to 2.35 µM at 30 m (Fig. 2; Table S4). Similar depth profiles were found for other heavy
348 elements as well, including Cu, Sr, Ba or Pb among others.

349 In the first 12 cm of sediments, DIC concentration in the porewater varied between ~ 21 and 26 mM, and δ¹³C_{DIC}
350 was around 0 ‰. Carbonates corresponded to aragonite and calcite and had a bulk C isotope composition between
351 2.1 and 2.6 ‰ (Table S3). Sedimentary organic matter had a δ¹³C_{SOC} averaging -26.8 ± 0.1 ‰ and a C:N molar
352 ratio increasing from 8 to 10 (Figs. 3, 4; Table S3).

353

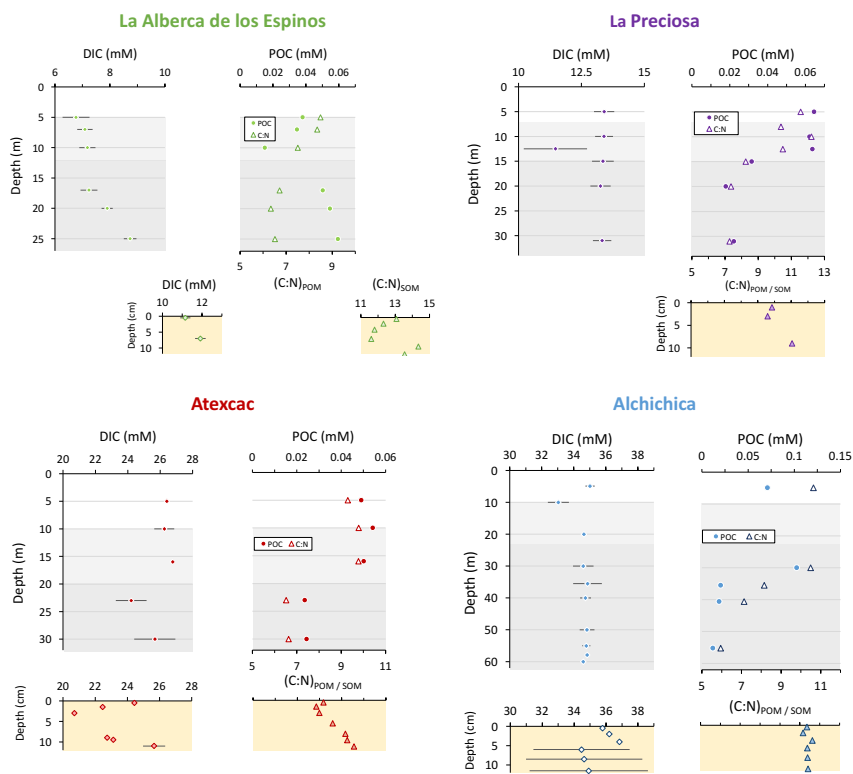


Figure 3. Concentrations in mmol/L (mM) of DIC, DOC, POC and sum of all three reservoirs, C:N molar ratios of POM as a function of depth in the water columns, as well as DIC concentrations in the surficial sediment porewaters and C:N molar ratios of sedimentary OM. Porewaters from La Preciosa's 2016 core were not retrieved.

354

355 4.4. Lake Alchichica

356 The water column of Lake Alchichica showed a pronounced stratification compared to previous years at the same
 357 period (Fig. 2, Fig. S2; Lugo et al., 2000; Adame et al., 2008; Macek et al., 2020). Temperature decreased from
 358 ~ 20 °C at the surface to 15.5 °C at depths below 30 m. Conductivity showed the same trend with values between
 359 around 13.8 mS/cm (salinity decreasing from 7.9 to 7.8 psu). Dissolved O₂ was slightly oversaturated at the lake
 360 surface (112 % or 7.5 mg/L), rapidly decreasing to 0 mg/L between ~ 10 and 20 m. The ORP followed a similar
 361 trend but decreasing below 30 m only. The offset between O₂ exhaustion and decrease of the ORP can be explained
 362 by the presence of other oxidant species and/or extended Chl a peaks (supplementary text 1). Chl a averaged
 363 2 µg/L, with a broad peak extending from ~ 7 to 29 m (averaging 4 µg/L and showing a narrow 6 µg/L maximum
 364 values at 23 m. Then, it decreased to minimum values of ~ 0.5 µg/L in the lower water column. The pH remained
 365 constant at ~9.2 over the whole water column. Based on the temperature profiles, the epi-, meta- and hypolimnion
 366 layers of Lake Alchichica in May 2019 extended from 0-10, 10-20 and 20-63 m, respectively (Fig. 2).

367 The DIC concentration was around 34.8 mM throughout the water column, except at 10 m where it decreased to
 368 33 mM (Fig. 3; Table S1). Calculated pCO_2 was about three times higher than the atmospheric pCO_{2atm} (Table S2).
 369 The $\delta^{13}C_{DIC}$ decreased from 2 to ~ 1.5 ‰ between 5 and 60 m depth (Fig. 4; Table S1). The POC concentration
 370 was ~ 0.09 mM in the epi-/metalimnion, decreasing to 0.02 mM in the hypolimnion. The $\delta^{13}C_{POC}$ increased from
 371 -26.5 ‰ in the top 30 m to -24.1 ‰ at 55 m. The C:N molar ratio of POM showed a similar profile with values
 372 around 10.5 down to 30 m, progressively decreasing towards 5.9 at 55 m (Fig. 3; Table S1).

373 In the first 12 cm of sediments, porewater DIC had a concentration of ~ 35.5 mM and $\delta^{13}C_{DIC}$ decreased from 0.4
 374 to -0.5 ‰. Solid carbonates were contained within several phases (aragonite, hydromagnesite, huntite and calcite)
 375 and had a bulk C isotope composition around 4.6 ‰ (Table S3). Sedimentary organic matter had a $\delta^{13}C_{SOC}$
 376 increasing from -25.7 to -24.5 ‰ and a constant C:N molar ratio slightly higher than 10 (Figs. 3, 4; Table S3).

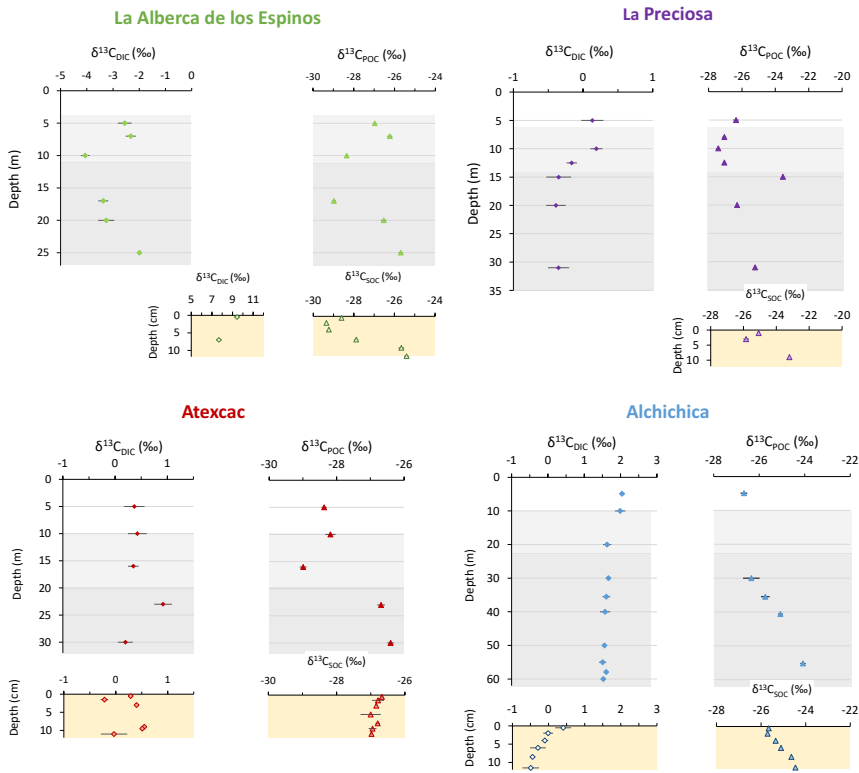


Figure 4. Isotopic compositions of DIC and POC reservoirs as a function of depth in the water columns, as well as isotopic compositions of the porewater-DIC and total organic carbon from the surficial sediments.

377

378

379 **5. DISCUSSION**

380

381 **5.1. Inorganic Carbon: origins and implications of the alkalinity/DIC gradient**

382

383 **5.1.1 Sources of DIC and origin of the inter-lake alkalinity gradient**

384 Salinity and DIC concentration gradually increase from La Alberca de los Espinos (0.6 psu, 7 mM) to Alchichica
385 (7.9 psu, 35 mM), while La Preciosa (1.15 psu, 13 mM) and Atexcac (7.44 psu, 26 mM) have intermediate values
386 (Table 1 and S1). This trend matches the alkalinity gradient (with values of ~ 8, 15, 32 and 47 meq/L, Fig. S3a)
387 previously described for these lakes (Zeyen et al., 2021), consistent with the fact that alkalinity is mainly composed
388 of HCO₃⁻ and CO₃²⁻ ions in most natural waters. This alkalinity gradient may result from different concentration
389 stages of an initial dilute alkaline water (Zeyen et al., 2021), ultimately controlled by differences in hydrological
390 regime between the four lakes. In the SOB, the weathering of basaltic/andesitic bedrock (Armieta et al., 2008;
391 Carrasco-Núñez et al., 2007; Lelli et al., 2021) and Cretaceous limestone (with δ¹³C ≈ 0 ± 1 ‰; Gonzales-Partida
392 et al., 1993; Armstrong-Altrin et al., 2011) favors the inflow of more alkaline and DIC-concentrated groundwater
393 than in La Alberca, which lies on an essentially basaltic basement (Rendon-Lopez, 2008; Siebe et al., 2014; Zeyen
394 et al., 2021). The SOB is currently experiencing higher rates of evaporation than precipitation (Alcocer, 2021),
395 which may play an important role in concentrating solutes and decreasing the water level in La Preciosa, Atexcac,
396 and Alchichica (Anderson and Stedmon, 2007; Zeyen et al., 2021). Substantial “sub-fossil” microbialite deposits
397 emerge well above the current water level in lakes Atexcac and Alchichica, confirming this fall in water level
398 (~15 m for Atexcac, and ~5 m for Alchichica). Scattered patches of microbialites emerge at La Preciosa
399 (suggesting a water level decrease of ~6 m). By contrast, emerged microbialites are virtually absent in Lake La
400 Alberca de los Espinos (Fig. S1).

401 Additional local parameters such as variable groundwater paths and fluxes (Furian et al., 2013; Mercedes-Martín
402 et al., 2019; Milesi et al., 2020; Zeyen et al., 2021) most likely play a role in explaining some of the variation in
403 DIC concentration between lakes. La Preciosa’s water composition significantly differs from that of Atexcac, and
404 Alchichica, despite a similar geological context and climate (all are located within 50 km², Fig. 1). Groundwater
405 in the SOB area becomes more saline as it flows towards the center of the basin and through the crater lakes (Silva
406 Aguilera, 2019; Alcocer, 2021). Since groundwater flows through La Preciosa first, its ionic strength (including
407 DIC concentration) increases, as it enters Alchichica (Silva Aguilera, 2019; Alcocer, 2021; Lelli et al., 2021).
408 Different regimes of volcanic CO₂ degassing into these crater lakes may also contribute to variation in the C mass
409 balance and δ¹³C_{DIC} values between the four lakes. Near the lakes from the SOB area, geothermal fluids derived
410 from meteoric waters have been shown to interact with deep volcanic fluids as well as the calcareous basement
411 rocks (Peiffer et al., 2018; Lelli et al., 2021). In the water column of La Alberca, δ¹³C_{total} averages -4.8 ‰ (Havas
412 et al., submitted). This isotopic composition is very similar to signatures of mantle-CO₂ (Javoy et al., 1986; Mason
413 et al., 2017), which could buffer the overall C isotope composition of this lake. La Alberca is located on top of a
414 likely active normal fault (Siebe et al., 2012), favoring the ascent of volcanic gases.

415 Differences in the remineralization rate of organic carbon (OC) could also contribute to the heterogeneous DIC
416 content among the lakes. However, assuming that all OC from the lakes ultimately remineralized into DIC, it
417 would still represent only a small proportion of the total carbon (9 % for La Alberca, ~5 % for La Preciosa and
418 Alchichica, and 16 % for Atexcac, Havas et al., submitted). From an isotopic mass balance perspective, Lake La

Deleted: becomes more concentrated

420 Alberca exhibits more negative $\delta^{13}\text{C}_{\text{DIC}}$ (and $\delta^{13}\text{C}_{\text{carb}}$), slightly closer to OC signatures, whereas the $\delta^{13}\text{C}_{\text{DIC}}$ of the
421 three SOB lakes lie very far from OC isotopic signatures (Fig. 4). Dense vegetation surrounds La Alberca (Fig. S1),
422 making it the only lake in this study where OC respiration could be a significant source of inorganic C to the water
423 column (potentially influencing the P_{CO_2} , [DIC] and pH profiles described above).

424 In summary, a combination of very local and external environmental factors generates the contrasting water
425 chemistries of the lakes, notably a gradient in their alkalinity/[DIC]. This chemical variability stems from the exact
426 nature of the basement rocks, the distinct groundwater flow paths feeding the lakes, differences in evaporation
427 rates, and potentially different volcanic- CO_2 degassing regimes.

428

429 5.1.2 Influence of alkalinity on physico-chemical stratification in the four lakes

430 Stratified water columns can sustain strong physico-chemical gradients, where a wide range of biogeochemical
431 reactions impacting the C cycle can take place (e.g. Jézéquel et al., 2016). In the four lakes studied here, the
432 evolution of pH with depth exemplifies the interplay between the alkalinity gradient, the physico-chemical
433 stratification of the lakes, and their respective C cycle. The pH shows a stratified profile in La Alberca and La
434 Preciosa, but remains constant in Atexcac and Alchichica. The decline in pH at the oxycline of La Preciosa is
435 associated with the decrease in POC and chlorophyll a concentrations and $\delta^{13}\text{C}_{\text{DIC}}$ values, reflecting the impact of
436 oxygen respiration (i.e. carbon remineralization) at this depth (Figs. 2-4). In La Alberca, the surface waters are
437 markedly more alkaline than the bottom waters, with a two-step decrease in pH occurring at 8 m and 17 m (with a
438 total drop of 1.5 pH unit). As in La Preciosa, this pH decrease likely results from high OM respiration, although
439 input of volcanic acidic gases (e.g. dissolved CO_2 with $\delta^{13}\text{C} \sim -5\text{‰}$) might also contribute to the pH decrease in
440 the bottom waters, reflected by negative $\delta^{13}\text{C}_{\text{DIC}}$ signatures and an increase of [DIC] and conductivity in the
441 hypolimnion (Figs. 2 and 4). By contrast, while the same evidence for oxygen respiration ([POC], chlorophyll a)
442 can be detected in the other two lakes, it does not impact their pH profile in a similar way (Fig. 2). This result
443 suggests that the acidity generated by OM respiration (and possibly volcanic- CO_2 degassing) is buffered by the
444 much higher alkalinity measured in these two lakes.

445 External forcings such as lake hydrology and fluid sources thus impact the alkalinity buffering capacity of these
446 lakes and influence the vertical pH profile of the water columns, which is particularly important considering the
447 critical interplay between pH and biogeochemical reactions affecting the C cycle (e.g. Soetaert et al., 2007).

448

449 5.1.3 Sinks of DIC along the alkalinity gradient

450 Interplay between pH and sources of alkalinity/DIC in the lakes also has a strong impact on their C storage capacity
451 as it can result in different fluxes of the C sinks (inorganic and organic C precipitation / sedimentation, CO_2
452 degassing).

453 Alkaline pH can store large quantities of DIC because it favors the presence of HCO_3^- and CO_3^{2-} species over
454 H_2CO_3^* (the intermediate species between gaseous $\text{CO}_{2(\text{g})}$ and bi-/carbonate ions, defined here as the sum of H_2CO_3
455 and $\text{CO}_{2(\text{aq})}$). Carbonate and bicarbonate ions represent over 99% of total DIC in the four lakes (Table S2). In La

Deleted: these

Deleted: reactions

Deleted: . This

459 Alberca de los Espinos, the lake with the lowest DIC, the surface water pCO₂ is slightly lower than atmospheric
460 pCO_{2atm} (Table S2). By contrast, large amounts of CO₂ degas at the surface of the SOB lakes, as indicated by their
461 elevated surface water pCO₂, from 2 to 5 times higher than atmospheric pCO_{2atm} (Table S2). These **different CO₂**
462 **degassing potentials** are consistent with the notion that higher DIC concentrations favor CO₂ degassing through
463 higher pCO₂ (e.g. Duarte et al., 2008). Although La Alberca and Alchichica (the two endmembers of the alkalinity
464 gradient) have the same surface water pH, CO₂ degassing is three times higher at Alchichica, for a given value of
465 gas transfer velocity.

Deleted: observations

466 Another important C sink for these lakes is the precipitation of carbonate minerals, found in the microbialites and
467 lake sediments. Lake alkalinity and resulting mineral saturation index greatly influence the amount of C
468 precipitated from the lake waters. Although the four lakes are supersaturated with aragonite, calcite and the
469 precursor phase monohydrocalcite, they present highly contrasted amounts of carbonate deposits (Zeyen et al.,
470 2021). The occurrence of microbialites increases along the alkalinity gradient, with limited presence at La Alberca,
471 and more massive deposits at Atexcac and Alchichica (Zeyen et al., 2021; Fig. S1). Similarly, surficial sediments
472 contain only 16 wt. % for La Alberca, but from 40 to 62 wt. % carbonates for the SOB lakes (Table S3). Thus, the
473 SOB lakes seem to bury more C than La Alberca de los Espinos. Nonetheless, the data from May 2019 indicate
474 that La Alberca was the only one of the four lakes with a pCO₂ slightly lower than atmospheric pCO_{2atm}, thus
475 representing a net sink of C. Classifying the three other lakes as net C sources or sinks – notably in order to see
476 the influence of their respective position in the alkalinity gradient – will require a more detailed description of C
477 in- and out-fluxes since they all store and emit significant amounts of C (as organic and inorganic C deposits and
478 via CO₂ degassing, respectively). However, **such a C budget** is out of the scope of the present study.

Deleted: this

479

480 5.1.4 Isotopic signatures of inorganic C in the four lakes ($\delta^{13}\text{C}_{\text{DIC}}$ and $\delta^{13}\text{C}_{\text{Carbonates}}$)

481 The DIC isotopic composition of the lakes (between ~ -3 and +2 ‰ on average; Table S1) is consistent with the
482 DIC sources described above. The lower $\delta^{13}\text{C}_{\text{DIC}}$ in La Alberca is consistent with influence of remineralized OC
483 and/or volcanic CO₂. The $\delta^{13}\text{C}_{\text{DIC}}$ in the SOB lakes suggests groundwater $\delta^{13}\text{C}_{\text{DIC}}$ values resulting from the
484 dissolution of the Cretaceous limestone basement.

485 By controlling DIC speciation (H₂CO₃/CO_{2(aq)}, HCO₃⁻, CO₃²⁻), pH also strongly influences $\delta^{13}\text{C}_{\text{DIC}}$. Indeed, there
486 is a temperature-dependent fractionation of up to 10 ‰ between the different DIC species (Emrich et al., 1970;
487 Mook et al., 1974; Bade et al., 2004; Table S6). The Mexican lakes present $\delta^{13}\text{C}_{\text{DIC}}$ values that are common for
488 lakes with a pH around 9 (Bade et al., 2004), where DIC is dominated by HCO₃⁻. However, the pH values of the
489 four lakes studied here are too similar to explain the significant difference between their $\delta^{13}\text{C}_{\text{DIC}}$ (Fig. 4; $p=4.2\times 10^{-3}$
490 for La Preciosa and Atexcac, which have the closest $\delta^{13}\text{C}_{\text{DIC}}$). Part of the variability of $\delta^{13}\text{C}_{\text{DIC}}$ among the lakes
491 may result from their distinct evaporation stages, as the mean $\delta^{13}\text{C}_{\text{DIC}}$ values of the lakes broadly correlate with
492 their salinity/alkalinity (Fig. S3b). Evaporation generally increases the $\delta^{13}\text{C}_{\text{DIC}}$ of residual waters by increasing
493 lake pCO₂ and primary productivity, **which bolsters CO₂ degassing and organic C burial, both having low $\delta^{13}\text{C}$**
494 compared to DIC (e.g. Li and Ku, 1997; Talbot, 1990). Accordingly, the pCO₂ of La Alberca is lower than that of
495 the other lakes (Table S2). The $\delta^{13}\text{C}_{\text{DIC}}$ in lakes with lower DIC concentrations is expected to be more easily
496 influenced by exchanges with other carbon reservoirs, such as organic carbon (through photosynthesis/respiration),

Deleted: . This

Deleted: which

Deleted: e

502 or other DIC sources (e.g., depleted volcanic CO₂ or groundwater DIC), compared with buffered, high DIC lakes
 503 (Li and Ku, 1997). As a result, the low DIC/alkalinity concentration in La Alberca features the lowest δ¹³C_{DIC} of
 504 the four lakes, likely reflecting organic and/or volcanic C influence and thus higher responsiveness to
 505 biogeochemical processes of the inorganic C reservoir. By contrast, the three SOB lakes exhibit δ¹³C_{DIC} with less
 506 internal variability, with a maximum amplitude of 0.7 ‰ within a single water column.

507 Surficial sedimentary carbonates are in isotopic equilibrium with the δ¹³C_{DIC} of the water columns, within the
 508 uncertainty of δ¹³C_{DIC} measurement, and more specifically with the δ¹³C_{DIC} values at the oxycline/thermocline of
 509 the lakes (Tables S6 and S7). [The δ¹³C_{DIC} at equilibrium with carbonates](#) is estimated by correcting the carbonates
 510 C isotope composition (δ¹³C_{carb}) by the fractionation value between DIC and the different carbonate mineralogies
 511 (supplementary text S2). Therefore, the δ¹³C_{carb} also follows and reflects the alkalinity gradient, with the lowest
 512 δ¹³C_{carb} found in the surficial sediments of La Alberca (~ -1.5 ‰), intermediate values in La Preciosa and Atexcac
 513 (~ -2.5 ‰), and the highest values in Alchichica (~ +4.6 ‰) (Table S3).

514

515 In summary, although all four lakes present the same general structure and environmental conditions (i.e. tropical
 516 alkaline stratified crater lakes), external and local factors (e.g. hydrology, fluid sources, and stratification
 517 characteristics) result in contrasting water chemistry compositions, which have a critical impact on the physico-
 518 chemical depth profiles of each lake and their biogeochemical carbon cycle functioning. These external factors
 519 represent a first-order control on the size, isotopic composition, and responsiveness to biogeochemical processes
 520 of the inorganic C reservoir. Lakes with the highest alkalinity/DIC content will poorly record internal biological
 521 processes. Interestingly, C storage in mineral carbonates seems to be significant in watersheds where carbonate
 522 deposits pre-exist in the geological substratum (here, the Cretaceous limestone basement), providing more alkaline
 523 and C-rich sources.

524

Symbols	Mathematical Expression	Signification
δ ¹³ C _X	$\left(\frac{\left(\frac{^{13}\text{C}}{^{12}\text{C}} \right)_X}{\left(\frac{^{13}\text{C}}{^{12}\text{C}} \right)_{VPDB}} - 1 \right) * 1000$	Relative difference in ¹³ C: ¹² C isotopic ratio between a sample of a given C reservoir and the international standard "Vienna Pee Dee Bee", expressed in permil (‰). δ ¹³ C _{total} represents the weighted average of δ ¹³ C for all DIC and POC.
Δ ¹³ C _{X-Y}	$= \delta^{13}\text{C}_X - \delta^{13}\text{C}_Y \approx 1000 \ln \alpha_{X-Y}$	Apparent isotopic fractionation between two reservoirs 'X' and 'Y'. Difference between their measured C isotope compositions approximating the fractionation α in ‰.
ε _{X-CO2}	$= (\alpha_{X-CO2} - 1)1000 \approx \delta^{13}\text{C}_X - \delta^{13}\text{C}_{CO2}$	Calculated isotopic fractionation between a reservoir 'X' and CO _{2(aq)} . α _{X-CO2} is calculated as (δ ¹³ C _X +1000)/(δ ¹³ C _{CO2} +1000) where δ ¹³ C _X is measured and δ ¹³ C _{CO2} is computed based on DIC isotopic composition and speciation (see supplementary text S3).

525

Deleted: This

527 Table 2
528 Index for mathematical notations used in the text including C isotopic composition of a reservoir X ($\delta^{13}C_X$),
529 isotopic discrimination between the two carbon reservoirs X and Y ($\Delta^{13}C_{X-Y}$). In the main text, we report organic
530 C isotope discrimination *versus* both bulk DIC ($\Delta^{13}C_{POC-DIC}$) – in a way to facilitate studies intercomparison and
531 because it is the commonly reported raw measured data (Fry, 1996) – and calculated $CO_{2(aq)}$ (ϵ_{POC-CO_2}) in order to
532 discuss the intrinsic isotopic fractionations associated with the lakes metabolic diversity. All C isotope values and
533 fractionations are reported relative to the international standard VPDB (Vienna Pee Dee Belemnite).

534

535

536 5.2. Particulate organic carbon: from water column primary production to respiration recycling and 537 sedimentary organic matter

538

539 5.2.1. Particulate organic C sources

540 *Primary productivity by oxygenic photosynthesis in the upper water column*

541 The C:N ratios of water-column POM and bulk organic matter in the sediments of the four lakes ranged from 6 to
542 13 (Fig. 3), close to the phytoplankton Redfield but much lower than land plant ratios. Yet abundant vegetation
543 covers the crater walls of La Alberca and, to a lesser extent, of Atexcac, and some plant debris was found in the
544 sediment cores of these two lakes. Its analysis resulted in high C:N ratios (between 24 and 68), typical of plant
545 tissues and significantly higher than those of the bulk sediment and water column organic matter. Thus, the
546 allochthonous organic carbon in these two lakes does not significantly contribute to their bulk organic signal. All
547 four crater lakes are endorheic basins, with no surface water inflow or outflow, supporting the predominantly
548 autochthonous origin of organic carbon sources (Alcocer et al., 2014b), from planktonic autotrophic C fixation.

549 The importance of planktonic autotrophic C fixation as a major source of POC in the four lakes is further supported
550 by the assessment of the isotopic discrimination between DIC and organic biomass, expressed as $\Delta^{13}C_{POC-DIC}$ and
551 ϵ_{POC-CO_2} (Table 2). The $\Delta^{13}C_{POC-DIC}$ varies between ~ -29 and -23 ‰ (corresponding to ϵ_{POC-CO_2} between ~ -19 and
552 -13 ‰) throughout the four water columns, within the typical range of planktonic oxygenic phototrophs (Pardue
553 et al., 1976; Sirevag et al., 1977; Thomas et al., 2019). Yet these values exhibit variability – both within a single
554 water column (up to 4.5 ‰) and among the four lakes (up to 6 ‰, Figs. 4 and 5). The $\Delta^{13}C_{POC-DIC}$ variability may
555 reflect several abiotic and biotic factors.

556 Notably, lower DIC availability in La Alberca and La Preciosa probably makes the carboxylation step less limiting
557 during photosynthesis (e.g. O’Leary, 1988; Descolas-Gros and Fontugne, 1990; Fry, 1996), decreasing $|\epsilon_{POC-CO_2}|$
558 in these lakes (between 14.5 and 17.7 ‰ at the peak of Chl. a) compared with Atexcac and Alchichica (Fig. 5a;
559 between 17.5 and 19.2 ‰). Lower $CO_{2(aq)}$ availability and/or higher reaction rates result in transport-limited rather
560 than carboxylation-limited fixation, with smaller C isotope fractionation between POC and DIC (Pardue et al.,
561 1976; Zohary et al., 1994; Fry, 1996; Close and Henderson, 2020). The isotopic fractionation associated with
562 diffusion is much smaller than with carboxylation, and a higher proportion of the DIC entering the cells is
563 converted into organic biomass (e.g. Fogel and Cifuentes, 1993). We consistently notice a correlation among the

Deleted: All four crater lakes are endorheic basins, with no surface water inflow or outflow. The organic carbon sources are therefore predominantly autochthonous, resulting mainly from planktonic autotrophic C fixation. This is supported by

Deleted: that

Deleted: ranged from 6 to 12 in

Deleted: far

Deleted: from

Deleted: A

Deleted: those of

Deleted: ;

Deleted: observed and sampled

Deleted: from

Deleted: .

Deleted: They

Deleted: has

Deleted: ve

Deleted: in the surficial sediments (between 8 and 13) and water column (between 6 and 12) (Fig. 3).

Deleted: Moreover,

Deleted: a

Deleted: that

Deleted:

Deleted: are predominantly autochthonous

Deleted: resulting mainly

Deleted: his

590 lakes between $a(\text{CO}_2)_{\text{aq}}$ (or [DIC]) and $[\epsilon_{\text{POC-CO}_2}]$ at depths where oxygenic photosynthetic peaks (Fig. 6).
 591 Furthermore, La Alberca and La Preciosa are considered less oligotrophic than the two other lakes (Lugo et al.,
 592 1993; Vilaclara et al., 1993; Havas et al., submitted), with higher chlorophyll a contents and thus smaller $[\epsilon_{\text{POC-CO}_2}]$
 593 (Fig. 5). Higher water temperatures in La Alberca de los Espinos (by $\sim 3^\circ\text{C}$) could also partly contribute to a
 594 smaller $[\epsilon_{\text{POC-CO}_2}]$ in this lake (Sackett et al., 1965; Pardue et al., 1976; Descolas-Gros and Fontungne, 1990).

595 Unlike $\delta^{13}\text{C}_{\text{DIC}}$, organic carbon isotope signatures do not evolve linearly with the alkalinity/salinity gradient,
 596 suggesting other lake- and microbial-specific controls on these signatures. These controls include: diffusive or
 597 active uptake mechanisms, specific carbon fixation pathways, the fraction of intracellular inorganic carbon
 598 released out of the cells, cell size and geometry (Werne and Hollander, 2004 and references therein) and
 599 remineralization efficiency. Moreover, an increasing amount of isotopic data has evidenced a significant variability
 600 of the isotopic fractionation achieved by different purified RuBisCO enzymes ($\epsilon_{\text{RuBisCO}}$, Iñiguez et al., 2020), and
 601 even by a single RuBisCO form (Thomas et al., 2019). Thus, caution should be paid to the interpretation of the
 602 origin of small isotopic variations of the biomass in distinct environmental contexts because RuBisCO alone can
 603 be an important source of this variability (Thomas et al., 2019).

604

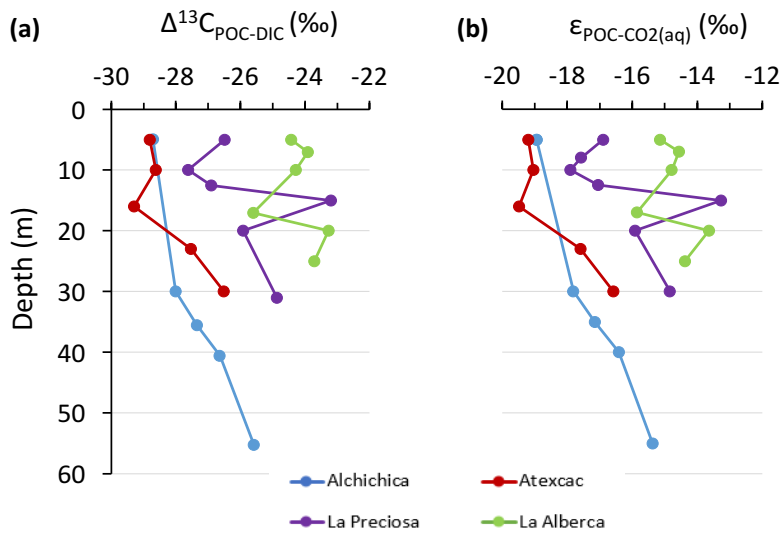


Figure 5. Isotopic fractionations between POC and DIC in the water columns of the four lakes, expressed as a) $\Delta^{13}\text{C}_{\text{x-y}}$ and b) $\epsilon_{\text{POC-CO}_2}$. Refer to Table 2 for more detail about the Δ and ϵ notations.

606 Anoxygenic autotrophs commonly thrive in anoxic
 607 bottom waters of stratified water bodies (e.g.
 608 Pimenov et al., 2008; Zyakun et al., 2009; Posth et
 609 al., 2017; Fulton et al., 2018; Havig et al., 2018).
 610 They have been identified at different depths in the
 611 four Mexican lakes (Macek et al., 2020; Iniesto et al.,
 612 2022). In our samples collected during the
 613 stratification period, anoxygenic autotrophs appear to
 614 have a distinct impact on the C cycle of La Alberca
 615 and Atexcac only. Lake Atexcac records a
 616 concomitant decrease in [DIC] and increase in
 617 $\delta^{13}\text{C}_{\text{DIC}}$ in the anoxic hypolimnion at 23 m, below the
 618 peak of Chl a, suggesting autotrophic C fixation by
 619 chemoautotrophy or anoxygenic photosynthesis. The
 620 calculated $\epsilon_{\text{POC-CO}_2}$ at 23 m (-17.3 ‰) is consistent
 621 with C isotope fractionation by purple- and green-
 622 sulfur-anoxygenic bacteria (PSB and GSB), while
 623 $\epsilon_{\text{POC-CO}_2}$ in La Alberca's hypolimnion (~ -15 ‰) is
 624 closer to GSB canonical signatures (Posth et al., 2017
 625 and references therein) (Fig. 5b). In La Alberca,
 626 anoxygenic primary productivity is suggested by
 627 increasing POC concentrations below the oxycline,
 628 showing a distinct isotopic signature (Figs. 4 and 5).
 629 We also observe a Chl a peak in the anoxic
 630 hypolimnion of this lake (Fig. 2), which likely
 631 represents a bias of the probe towards some
 632 bacteriochlorophyll pigments typical of GSB (see
 633 supplementary text S4). In Atexcac, C fixation by
 634 anoxygenic autotrophs at 23 m causes a shift in the DIC
 635 reservoir, while oxygenic photosynthesis at 16 m does
 636 not, suggesting that anaerobic autotrophs are the main
 637 autotrophic metabolisms in this lake (in terms of DIC
 638 uptake). In La Alberca, the increase in [POC] to
 639 maximum values below the oxycline also supports the
 640 predominance of anoxygenic *versus* oxygenic
 641 autotrophy (Fig. 3), similarly to other stratified water
 642 bodies exhibiting primary production clearly dominated
 643 by anoxygenic metabolisms (Fulton et al., 2018).

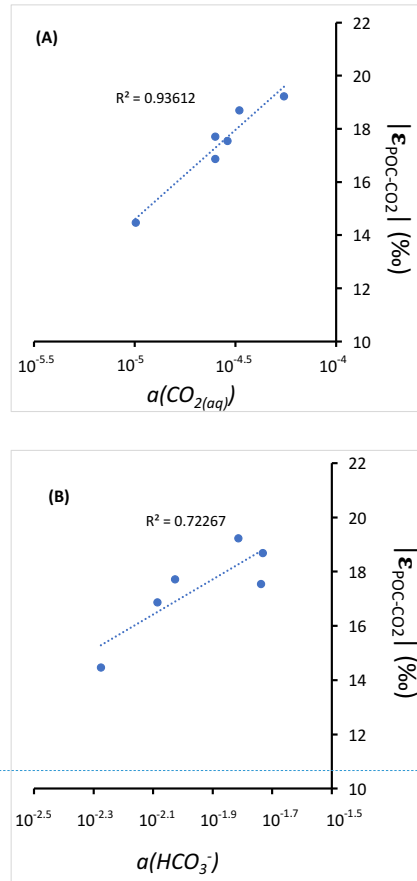


Figure 6.

Cross plots of DIC species activities *versus* absolute values of calculated C isotopic fractionations between POC and CO_2 at depths of peak oxygenic photosynthesis where data was available (5 and 30 m for Alchichica, 16 m for Atexcac, 10 and 12.5 m for La Preciosa and 7 m for La Alberca). (A) Dissolved $\text{CO}_2(\text{aq})$ activity and (B) bicarbonate activity as functions of $|\epsilon_{\text{POC-CO}_2}|$ in ‰ plus linear correlation trends and corresponding R^2 .

Deleted: and

Deleted: at depth

Deleted: . This is

647 Lastly, at 23 m in Atexcac and 17 m in La Alberca, we find a striking turbidity peak precisely where the redox
648 potential and the concentration of dissolved Mn drops (Fig. 2). In Atexcac, the concentration in dissolved metals
649 such as Cu, Pb, or Co also drops at 23 m (Fig. S4). In La Alberca, a peak of particulate Mn concentration is detected
650 at 15 m (Fig. 2; data unavailable for Atexcac). This peak is most likely explained by the precipitation of Mn mineral
651 particles, where reduced bottom waters meet oxidative conditions prevailing in the upper waters. These oxidized
652 Mn phases can be used as electron acceptors during chemoautotrophy (Havig et al., 2015; Knossow et al., 2015;
653 Henkel et al., 2019; van Vliet et al., 2021). Even at a low particle density, such phases can catalyze abiotic oxidation
654 of sulfide to sulfur compounds, which in turn can be used and further oxidized to sulfate by phototrophic or
655 chemoautotrophic sulfur-oxidizing bacteria (van Vliet et al., 2021). ~~Autotrophic sulfur oxidation~~ is also consistent
656 with the small increase in $[\text{SO}_4^{2-}]$ observed at 23 m in Atexcac (Table S4).

Deleted: This

657 In summary, combined POC and DIC data allowed us to recognize the most representative autotrophic
658 metabolisms in the Mexican lakes. The upper water columns are all dominated by oxygenic photosynthesis. Lower
659 in the water columns, anoxygenic photosynthesis and/or chemoautotrophy were found to have a noticeable impact
660 on POC and DIC reservoirs in La Alberca and Atexcac only. Their activity was associated with metal elements
661 cycling. More specifically in La Alberca, the anoxygenic phototrophs correspond to GSB.

662
663

664 5.2.2. Sinks of particulate organic carbon: respiration and sedimentation

665 *Aerobic respiration at the oxycline*

666 At the oxycline of stratified water bodies, aerobic respiration of OM by heterotrophic organisms favors the
667 transition from oxygenated upper layers to anoxic bottom waters. In the water column of the four lakes, $\Delta^{13}\text{C}_{\text{POC-DIC}}$
668 (and $\epsilon_{\text{POC-CO}_2}$) show increasing values in the hypolimnion, and especially below the chlorophyll a peaks (Figs. 2
669 and 5). ~~The $\Delta^{13}\text{C}_{\text{POC-DIC}}$ trend correlates with increasing $\delta^{13}\text{C}_{\text{POC}}$, decreasing (C:N)_{POM} ratios as well as decreasing~~
670 POC concentrations except in La Alberca (Figs. 3 and 4). Decreasing POC concentrations near the oxycline and
671 redoxcline are consistent with the fact that part of the upper primary production is degraded deeper in the water
672 columns and/or that there is less primary production in the anoxic bottom waters. Increased $\delta^{13}\text{C}_{\text{POC}}$ in the
673 hypolimnion of the lakes is consistent with heterotrophic activity and points out that POC at these depths could
674 mainly record secondary production rather than being a residue of sinking degraded OM formed by primary
675 production. Heterotrophic bacteria preferentially grow on available ^{13}C -enriched amino acids and sugars, thus
676 becoming more enriched than their C source (Williams and Gordon, 1970; Hayes et al., 1989; Zohary et al., 1994;
677 Briones et al., 1998; Lehmann et al., 2002; Jiao et al., 2010; Close and Henderson, 2020). The decrease in C:N
678 ratios in the POM also reinforces this conclusion since secondary heterotrophic bacteria biomass generally have
679 C:N between 4 and 5 (Lehmann et al., 2002), whereas residual degraded OM from primary producers would carry
680 higher C:N signatures (van Mooy et al., 2002; Buchan et al., 2014). These latter signatures are not recorded by
681 POM in the lower water columns of the lakes (Fig. 3).

Deleted: This

Deleted: also

682 The $\delta^{13}\text{C}_{\text{DIC}}$ signatures in La Preciosa and Alchichica are consistent with the mineralization of OM as they exhibit
683 lower values below the oxycline than in surficial waters (Figs. 2 and 4). Similarly to what is observed in several
684 other water bodies and notably stratified water columns such as the Black Sea (e.g. Fry et al., 1991), surface

688 photosynthesis increases $\delta^{13}\text{C}_{\text{DIC}}$ by fixing light DIC, while respiration transfers light OC back to the DIC pool at
689 depth. Such a decrease in $\delta^{13}\text{C}_{\text{DIC}}$ can also be seen in the oxycline of Lake La Alberca between 7 and 10 m.

690
691 *Influence of methanogenesis in Lake La Alberca de los Espinos*

692 La Alberca shows the least saline/alkaline water column and most peculiar geochemical depth profiles among the
693 four lakes. Notably, its [DIC] and $\delta^{13}\text{C}_{\text{DIC}}$ (the lowest of the studied lakes) increase from the lower metalimnion to
694 the hypolimnion, and further into the first cm of sediment porewaters, with $\delta^{13}\text{C}_{\text{DIC}}$ reaching almost 10 ‰ (Figs. 3;
695 4). The calculated CO_2 partial pressure (P_{CO_2}) increases downward from slightly less than $1 \times P_{\text{CO}_2\text{-atm}}$ near the lake
696 surface up to almost 40x at the bottom of the lake (Table S2).

697 While the increase of [POC] at depth may contribute to the observed $\delta^{13}\text{C}_{\text{DIC}}$ increase, by mass balance, it should
698 also lower the [DIC] instead of increasing it. Similarly, the sinking of POC at depth followed by its
699 remineralization into DIC cannot explain ~~the $\delta^{13}\text{C}_{\text{DIC}}$ trend~~, since it would lower the $\delta^{13}\text{C}_{\text{DIC}}$ in the hypolimnion
700 (Fig. 4). Overall, these observations require that a significant source of inorganic ^{13}C -rich carbon fuels the bottom
701 waters of La Alberca de los Espinos. The source of heavy carbon most likely results from methanogenesis, which
702 consumes organic carbon in the sediments and produces ^{13}C -depleted methane and ^{13}C -rich carbon dioxide
703 diffusing upward in the water column (i.e. acetoclastic methanogenesis, dominant in lacustrine contexts, Whiticar
704 et al., 1986). Methanogenesis, as an “alternative” OM remineralization pathway would be favored in La Alberca,
705 because it is relatively rich in OM (notably with high [DOC], Havas et al., submitted), and depleted in SO_4^{2-}
706 (Wittkop et al., 2014; Birgel et al., 2015; Cadeau et al., 2020) compared with the three other Mexican lakes. Based
707 on the $\delta^{13}\text{C}_{\text{SOC}}$ and porewater $\delta^{13}\text{C}_{\text{DIC}}$, we can tentatively calculate the methane isotopic signature in La Alberca
708 (see supplementary text S5). The resulting $\delta^{13}\text{C}_{\text{CH}_4}$ in the first 10 cm of sediments is between -59 and -57 ‰, which
709 is consistent with the range of isotopic composition of methane after biogenic methanogenesis (Whiticar et al.,
710 1986).

711 Upward diffusing methane may be either (i) partly lost from the lake’s surface (i.e. escaping the system) by
712 degassing or (ii) totally retained in the water column by complete oxidation (either abiotically by oxygenated
713 surface waters or biologically by methanotrophic organisms). The oxidation of CH_4 in the water column should
714 lead to the formation of ^{13}C -depleted carbon dioxide that would mix back with the lake DIC (and notably with
715 heavy methanogenic CO_2 produced at depth) and/or ^{13}C -depleted biomass (as POC or SOC) if it occurs through
716 methanotrophy. Thus, the net effect of combined methanogenesis and methane oxidation is expected to (i) generate
717 a $\delta^{13}\text{C}_{\text{DIC}}$ gradient from high to low values between the sediment porewaters and the oxycline as proposed
718 elsewhere (Assayag et al., 2008; Wittkop et al., 2014) and (ii) progressively lower sedimentary $\delta^{13}\text{C}_{\text{SOC}}$ in the case
719 of methanotrophy. Abiotic oxidation of methane by dioxygen is consistent with the observation that $\delta^{13}\text{C}_{\text{DIC}}$
720 decreases from porewaters ($\sim +10$ ‰) to the oxycline (-4 ‰), reaching minimum values where dissolved- O_2 starts
721 to appear (Fig. 2). Microbial anaerobic oxidation of methane (AOM) could occur at the 17 m depth through Mn-
722 oxide reduction (Cai et al., 2021; Cheng et al., 2021) and possibly bacterial sulfate-reduction closer to the water-
723 sediment interface, as inferred for the surficial sediments of meromictic Lake Cadagno (Posth et al., 2017). Indeed,
724 we observe a net increase of particulate Fe and S concentrations at a depth of 25 m and a peak of solid sulfide
725 minerals in the surficial sediments (Fig. S5). However, $\delta^{13}\text{C}_{\text{SOC}}$ and $\delta^{13}\text{C}_{\text{POC}}$ are far from calculated $\delta^{13}\text{C}_{\text{CH}_4}$,

Deleted: these

Deleted: observations

728 suggesting that AOM is not a major process in the bottom lake waters and surface sediments (Lehmann et al.,
729 2004) and thus that methanotrophy is not the main CH₄ oxidation pathway in Lake La Alberca.

730 Alternatively, if some portion of the methane escaped oxidation and degassed out of the lake, δ¹³C_{DIC} would likely
731 be driven to extreme positive values with time (Gu et al., 2004; Hassan, 2014; Birgel et al., 2015; Cadeau et al.,
732 2020). ~~Methane escape is not consistent with the average δ¹³C_{DIC} in La Alberca (~-3 ‰; Fig. 4), unless an~~
733 additional counterbalancing source of DIC to this lake exists. This source of DIC could be volcanic CO₂-degassing
734 (see section 5.1.1). Such a contribution may maintain the lake's average δ¹³C_{total} close to a mantle isotopic signature
735 and notably away from extreme positive values if CH₄-escape dominated. It is also possible that volcanic CO₂
736 degassing is coupled to methanogenesis by CO₂ reduction in addition to the acetoclastic type described above.

737 Although volcanic CO₂ could be an important source in the C mass balance of Lake La Alberca, we note that it
738 cannot explain the very positive δ¹³C_{DIC} in the sediment porewaters alone, thus bolstering the identification of
739 methanogenesis. Importantly, this methane cycle is cryptic to the sediment record, as it is evidenced in the
740 dissolved inorganic C phase, but not in the sedimentary organic matter or carbonates. This is a consequence of the
741 lake's stratified nature, where the location of carbonate precipitation and methane production is decoupled.

742

743 *Transfer of OM from the water column to the surficial sediments*

744 The OC content in the first 12 cm of the sediment cores from the four lakes ranges from 1 to 13 wt. % (Table S3).
745 ~~These concentrations are relatively elevated considering the predominantly autochthonous nature of OC and the~~
746 oligotrophic conditions in these lakes (Alcocer et al., 2014; Havas et al., submitted). In Lake Alchichica, the recent
747 OC burial flux in the sediment was estimated to represent between 15 and 26 g.yr⁻¹.m⁻² (Alcocer et al., 2014).
748 ~~These values are~~ within the range observed for small lakes around the world (Mulholland and Elwood, 1982; Dean
749 and Gorham, 1998; Mendonça et al., 2017), though most of them receive allochthonous OM inputs. Different
750 factors can favor the preservation of OM including lower respiration and oxidation rates due to anoxic bottom
751 waters and scarce benthic biota and/or high sedimentation rates (Alcocer et al., 2014). Anaerobic respiration clearly
752 occurs in the four lakes to some extent, as detailed for La Alberca, and as seen in the surficial sediment data of the
753 other lakes as well (decreasing δ¹³C_{DIC} in Alchichica, increasing C:N ratio in Atexcac and La Preciosa; Table S3).
754 Nonetheless, the anoxic conditions prevailing in the hypolimnion most of the year are significantly more favorable
755 to OM preservation than oxic conditions (Sobek et al., 2009; Kuntz et al., 2015). While the yearly mixing oxidizes
756 most of the water column during the winter, it also generates a bloom of diatoms which fosters OM production
757 (through shuttling up of bio essential nutrient such as N and Si) and development of anoxia (e.g. Adame et al.,
758 2008). In Alchichica, the large size of some of the phytoplankton was also suggested to favor OM preservation
759 (Adame et al., 2008; Ardiles et al., 2011). Because bacterial sulfate reduction (BSR) is a major remineralization
760 pathway in SO₄-rich environments (e.g. Jørgensen, 1982), the low sulfate content in La Alberca probably favors
761 the preservation of high TOC in the sediments. Even though, appreciable BSR rates may occur in this lake (see
762 discussion above and Fig. S5), similarly to other sulfate-poor environments due to rapid S-cycling (e.g. Vuillemin
763 et al., 2016; Friese et al., 2021). Again, a complete mass-balance of these lakes C fluxes will be required to estimate
764 their net C emission or sequestration behavior.

Deleted: This

Formatted: French

Deleted: This

Deleted: appears to be

Deleted: his

Deleted: is

Deleted: of values

771 Although the nature and geochemical signatures of the OM that deposits in the sediments may vary throughout the
772 year, it is interesting to infer from what part(s) of the water column surficial sedimentary OM comes during the
773 stratified seasons. In the three lakes from the SOB, $\delta^{13}\text{C}_{\text{SOC}}$ and $(\text{C:N})_{\text{SOM}}$ signatures of the surficial sedimentary
774 OM lie somewhere between POM signatures from the upper water column and from the hypolimnion (Figs. 3, 4).
775 More precisely, in Alchichica, the most surficial $\delta^{13}\text{C}_{\text{SOC}}$ and $(\text{C:N})_{\text{SOM}}$ signatures (-25.7 ‰ and 10.4, respectively)
776 are much closer to values recorded in the upper water column (~ -26.5 ‰ and 10.5, respectively), implying that
777 the upper oxygenic photosynthesis production is primarily recorded. It is consistent with previous studies
778 suggesting that most of the phytoplankton biomass being exported is composed of diatoms (Ardiles et al., 2011).
779 In Lake Atexcac, however, $\delta^{13}\text{C}_{\text{SOC}}$ and $(\text{C:N})_{\text{SOM}}$ signatures (~ -26.8 ‰ and 8, respectively) are closer to values
780 recorded in the hypolimnion (~ -26.5 ‰ and 6.5, respectively) suggesting that SOM records mostly the anaerobic
781 primary production.

782 In La Alberca, surficial $\delta^{13}\text{C}_{\text{SOC}}$ is markedly more negative (by ~ 2 to 3 ‰) than the deepest and shallowest water
783 column values (Fig. 4), but close to what is recorded at the redoxcline depth of 17 m. However, the $(\text{C:N})_{\text{SOM}}$
784 values are much higher than what is measured anywhere in the water column, which is consistent with OM
785 remineralization by sulfate-reduction and methanogenesis in the sediments of this lake. Therefore, OM
786 biogeochemical signatures in the surficial sediments of La Alberca could be strongly influenced by early diagenesis
787 occurring at the water-sediment interface – despite favorable conditions for OM preservation.

788 ~~In summary, the~~ OM depositing at the bottom of these stratified lakes does not always record geochemical
789 signatures from the same layers of the water columns and can be modified by very early diagenesis. It does not
790 necessarily record the signatures of primary production by oxygenic photosynthesis from the upper column. For
791 example, in Lake Atexcac, sedimentary OM records primary production by anoxygenic photosynthesis, even
792 though POC concentration is highest in the upper water column. This [result](#) highlights the diversity of geochemical
793 signatures that can stem from continental environments despite their geographical, geological, and climatic
794 proximity. A deeper understanding of the OM transfer process from water column to sediment will require more
795 detailed analyses and comparison of the different OM pigments and molecules and could have strong implications
796 for the interpretation of the fossil record in deep anoxic time.

797

798 6. CONCLUSIONS AND SUMMARY

799 The carbon cycles of four stratified alkaline crater lakes were described and compared based on the concentration
800 and isotopic compositions of DIC and POC in the water columns and surficial (~10 cm) sedimentary carbonates
801 and organic carbon. Overall our study shows the wide diversity of geochemical signatures found in continental
802 stratified environments despite similar geological and climatic contexts. We identify different regimes of C cycling
803 in the four lakes due to different biogeochemical reactions related to slight environmental and ecological
804 variations. In more detail, we show that:

- 805 - External abiotic factors, such as the hydrological regime and the inorganic C sources in the lakes, control
806 their alkalinity and thus, the buffering capacity of their waters. In turn, these differences in buffering
807 capacity constrain variations in pH along the stratified water columns as well as the inorganic C isotope
808 signatures recorded in the water columns and sediments of the lakes. The $\delta^{13}\text{C}_{\text{carb}}$ reflects the abiotic

Deleted: Overall

Deleted: this

Deleted: suggests that

812 factors generating the alkalinity gradient, but it is poorly representative of biological processes in lakes
813 with high alkalinity. The external environmental factors further impact the C mass balance of the lakes
814 with probable consequences on their net C-emitting or -sequestering status.

- 815 - Based on POC and DIC concentrations and isotopic compositions, combined with physico-chemical
816 parameters, we are able to identify the activity of oxygenic photosynthesis and aerobic respiration in the
817 four lakes studied. Anoxygenic photosynthesis and/or chemoautotrophy are also evidenced in two of the
818 lakes, but their POC and DIC signatures can be equivocal.
- 819 - Methanogenesis is evidenced in the surficial sediments of the OM-rich Lake La Alberca de los Espinos
820 and influences the geochemical signatures lower in the water column. However, it is recorded only in
821 analyses of porewater dissolved species, but not imprinted in the sedimentary archives (OM and
822 carbonates).
- 823 - The SOM geochemical signatures of these stratified lakes do not all record the same “biogeochemical
824 layers” of the water column (e.g. anaerobic vs. aerobic metabolisms), and, in some cases, can be greatly
825 modified by early diagenesis.

826

827 **Author Contributions**

828 RH and CT designed the study in a project directed by PLG, KB and CT. CT, MI, DJ, DM, RT, PLG and KB
829 collected the samples on the field. RH carried out the measurements for C data; DJ the physico-chemical parameter
830 probe measurements and EM provided data for trace and major elements. RH and CT analyzed the data. RH wrote
831 the manuscript with important contributions of all co-authors.

832

833 **Competing Interests**

834 The authors declare that they have no conflict of interest.

835

836 **Disclaimer**

837

838 **Acknowledgements**

839 This work was supported by Agence Nationale de la Recherche (France; ANR Microbialites, grant number ANR-
840 18-CE02-0013-02). The authors thank Anne-Lise Santoni, Elodie Cognard, Théophile Cocquerez and the GISMO
841 platform (Biogéosciences, Université Bourgogne Franche-Comté, UMR CNRS 6282, France). We thank Céline
842 Liorzou and Bleuenn Guéguen for the analyses at the Pôle Spectrométrie Océan (Laboratoire Géo-Océan, Brest,
843 France) and Laure Cordier for ion chromatography analyses at IPGP (France). We thank Nelly Assayag and Pierre
844 Cadeau for their help on the AP 2003 at IPGP.

845

846 **References**

847 Adame, M.F., Alcocer, J., Escobar, E., 2008. Size-fractionated phytoplankton biomass and its
848 implications for the dynamics of an oligotrophic tropical lake. *Freshw. Biol.* 53, 22–31.
849 <https://doi.org/10.1111/j.1365-2427.2007.01864.x>

850 Ader, M., Macouin, M., Trindade, R.I.F., Hadrien, M.-H., Yang, Z., Sun, Z., Besse, J., 2009. A
851 multilayered water column in the Ediacaran Yangtze platform? Insights from carbonate and organic
852 matter paired $\delta^{13}\text{C}$. *Earth Planet. Sci. Lett.* 288, 213–227. <https://doi.org/10.1016/j.epsl.2009.09.024>

853 Aharon, P., 2005. Redox stratification and anoxia of the early Precambrian oceans: Implications for
854 carbon isotope excursions and oxidation events. *Precambrian Res.* S0301926805000355.
855 <https://doi.org/10.1016/j.precamres.2005.03.008>

856 Alcocer, J., 2021. *Lake Alchichica Limnology*, Springer Nature. ed.

857 Alcocer, J., Ruiz-Fernández, A.C., Escobar, E., Pérez-Bernal, L.H., Oseguera, L.A., Ardiles-Gloria, V.,
858 2014. Deposition, burial and sequestration of carbon in an oligotrophic, tropical lake. *J. Limnol.* 73.
859 <https://doi.org/10.4081/jlimnol.2014.783>

860 Anderson, N.John., Stedmon, C.A., 2007. The effect of evapoconcentration on dissolved organic
861 carbon concentration and quality in lakes of SW Greenland. *Freshw. Biol.* 52, 280–289.
862 <https://doi.org/10.1111/j.1365-2427.2006.01688.x>

863 Ardiles, V., Alcocer, J., Vilaclara, G., Oseguera, L.A., Velasco, L., 2012. Diatom fluxes in a tropical,
864 oligotrophic lake dominated by large-sized phytoplankton. *Hydrobiologia* 679, 77–90.
865 <https://doi.org/10.1007/s10750-011-0853-7>

866 Armienta, M.A., Vilaclara, G., De la Cruz-Reyna, S., Ramos, S., Cenicerros, N., Cruz, O., Aguayo, A.,
867 Arcega-Cabrera, F., 2008. Water chemistry of lakes related to active and inactive Mexican volcanoes.
868 *J. Volcanol. Geotherm. Res.* 178, 249–258. <https://doi.org/10.1016/j.jvolgeores.2008.06.019>

869 Armstrong-Altrin, J.S., Madhavaraju, J., Sial, A.N., Kasper-Zubillaga, J.J., Nagarajan, R., Flores-Castro,
870 K., Rodríguez, J.L., 2011. Petrography and stable isotope geochemistry of the cretaceous El Abra
871 Limestones (Actopan), Mexico: Implication on diagenesis. *J. Geol. Soc. India* 77, 349–359.
872 <https://doi.org/10.1007/s12594-011-0042-3>

873 Assayag, N., Jézéquel, D., Ader, M., Viollier, E., Michard, G., Prévot, F., Agrinier, P., 2008. Hydrological
874 budget, carbon sources and biogeochemical processes in Lac Pavin (France): Constraints from $\delta^{18}\text{O}$
875 of water and $\delta^{13}\text{C}$ of dissolved inorganic carbon. *Appl. Geochem.* 23, 2800–2816.
876 <https://doi.org/10.1016/j.apgeochem.2008.04.015>

877 Assayag, N., Rivé, K., Ader, M., Jézéquel, D., Agrinier, P., 2006. Improved method for isotopic and
878 quantitative analysis of dissolved inorganic carbon in natural water samples. *Rapid Commun. Mass*
879 *Spectrom.* 20, 2243–2251. <https://doi.org/10.1002/rcm.2585>

880 Bade, D.L., Carpenter, S.R., Cole, J.J., Hanson, P.C., Hesslein, R.H., 2004. Controls of $\delta^{13}\text{C}$ -DIC in lakes:
881 Geochemistry, lake metabolism, and morphometry. *Limnol. Oceanogr.* 49, 1160–1172.
882 <https://doi.org/10.4319/lo.2004.49.4.1160>

883 Bekker, A., Holmden, C., Beukes, N.J., Kenig, F., Eglinton, B., Patterson, W.P., 2008. Fractionation
884 between inorganic and organic carbon during the Lomagundi (2.22–2.1 Ga) carbon isotope excursion.
885 *Earth Planet. Sci. Lett.* 271, 278–291. <https://doi.org/10.1016/j.epsl.2008.04.021>

886 Birgel, D., Meister, P., Lundberg, R., Horath, T.D., Bontognali, T.R.R., Bahniuk, A.M., de Rezende, C.E.,
887 Vasconcelos, C., McKenzie, J.A., 2015. Methanogenesis produces strong ^{13}C enrichment in
888 stromatolites of Lagoa Salgada, Brazil: a modern analogue for Palaeo-/Neoproterozoic stromatolites?
889 *Geobiology* 13, 245–266. <https://doi.org/10.1111/gbi.12130>

890 Briones, E.E., Alcocer, J., Cienfuegos, E., Morales, P., 1998. Carbon stable isotopes ratios of pelagic
891 and littoral communities in Alchichica crater-lake, Mexico. *Int. J. Salt Lake Res.* 7, 345–355.
892 <https://doi.org/10.1007/BF02442143>

893 Buchan, A., LeClerc, G.R., Gulvik, C.A., González, J.M., 2014. Master recyclers: features and functions
894 of bacteria associated with phytoplankton blooms. *Nat. Rev. Microbiol.* 12, 686–698.
895 <https://doi.org/10.1038/nrmicro3326>

896 Cadeau, P., Jézéquel, D., Leboulanger, C., Fouilland, E., Le Floch, E., Chaduteau, C., Milesi, V.,
897 Guélard, J., Sarazin, G., Katz, A., d'Amore, S., Bernard, C., Ader, M., 2020. Carbon isotope evidence for
898 large methane emissions to the Proterozoic atmosphere. *Sci. Rep.* 10, 18186.
899 <https://doi.org/10.1038/s41598-020-75100-x>

900 Cai, C., Li, K., Liu, D., John, C.M., Wang, D., Fu, B., Fakhraee, M., He, H., Feng, L., Jiang, L., 2021.
901 Anaerobic oxidation of methane by Mn oxides in sulfate-poor environments. *Geology* 49, 761–766.
902 <https://doi.org/10.1130/G48553.1>

903 Callieri, C., Coci, M., Corno, G., Macek, M., Modenutti, B., Balseiro, E., Bertoni, R., 2013. Phylogenetic
904 diversity of nonmarine picocyanobacteria. *FEMS Microbiol. Ecol.* 85, 293–301.
905 <https://doi.org/10.1111/1574-6941.12118>

906 Carrasco-Núñez, G., Ort, M.H., Romero, C., 2007. Evolution and hydrological conditions of a maar
907 volcano (Atexcac crater, Eastern Mexico). *J. Volcanol. Geotherm. Res.* 159, 179–197.
908 <https://doi.org/10.1016/j.jvolgeores.2006.07.001>

909 Chako Tchamabé, B., Carrasco-Núñez, G., Miggins, D.P., Németh, K., 2020. Late Pleistocene to
910 Holocene activity of Alchichica maar volcano, eastern Trans-Mexican Volcanic Belt. *J. South Am. Earth*
911 *Sci.* 97, 102404. <https://doi.org/10.1016/j.jsames.2019.102404>

912 Cheng, C., Zhang, J., He, Q., Wu, H., Chen, Y., Xie, H., Pavlostathis, S.G., 2021. Exploring simultaneous
913 nitrous oxide and methane sink in wetland sediments under anoxic conditions. *Water Res.* 194,
914 116958. <https://doi.org/10.1016/j.watres.2021.116958>

915 Close, H.G., Henderson, L.C., 2020. Open-Ocean Minima in $\delta^{13}\text{C}$ Values of Particulate Organic Carbon
916 in the Lower Euphotic Zone. *Front. Mar. Sci.* 7, 540165. <https://doi.org/10.3389/fmars.2020.540165>

917 Crowe, S.A., Katsev, S., Leslie, K., Sturm, A., Magen, C., Nomosatryo, S., Pack, M.A., Kessler, J.D.,
918 Reeburgh, W.S., Roberts, J.A., González, L., Douglas Haffner, G., Mucci, A., Sundby, B., Fowle, D.A.,
919 2011. The methane cycle in ferruginous Lake Matano: Methane cycle in ferruginous Lake Matano.
920 *Geobiology* 9, 61–78. <https://doi.org/10.1111/j.1472-4669.2010.00257.x>

921 Dean, W.E., Gorham, E., 1998. Magnitude and significance of carbon burial in lakes, reservoirs, and
922 peatlands. *Geology* 26, 535. [https://doi.org/10.1130/0091-7613\(1998\)026<0535:MASOCB>2.3.CO;2](https://doi.org/10.1130/0091-7613(1998)026<0535:MASOCB>2.3.CO;2)

923 Descolas-Gros, C., Fontugne, M., 1990. Stable carbon isotope fractionation by marine
924 phytoplankton during photosynthesis. *Plant Cell Environ.* 13, 207–218.
925 <https://doi.org/10.1111/j.1365-3040.1990.tb01305.x>

926 Emrich, K., Ehhalt, D.H., Vogel, J.C., 1970. Carbon isotope fractionation during the precipitation of
927 calcium carbonate. *Earth Planet. Sci. Lett.* 8, 363–371. [https://doi.org/10.1016/0012-821X\(70\)90109-3](https://doi.org/10.1016/0012-821X(70)90109-3)
928 3

- 929 Ferrari, L., Orozco-Esquivel, T., Manea, V., Manea, M., 2012. The dynamic history of the Trans-
930 Mexican Volcanic Belt and the Mexico subduction zone. *Tectonophysics* 522–523, 122–149.
931 <https://doi.org/10.1016/j.tecto.2011.09.018>
- 932 Fogel, M.L., Cifuentes, L.A., 1993. Isotope Fractionation during Primary Production, in: Engel, M.H.,
933 Macko, S.A. (Eds.), *Organic Geochemistry, Topics in Geobiology*. Springer US, Boston, MA, pp. 73–98.
934 https://doi.org/10.1007/978-1-4615-2890-6_3
- 935 Friese, A., Bauer, K., Glombitza, C., Ordoñez, L., Ariztegui, D., Heuer, V.B., Vuillemin, A., Henny, C.,
936 Nomosatryo, S., Simister, R., Wagner, D., Bijaksana, S., Vogel, H., Melles, M., Russell, J.M., Crowe,
937 S.A., Kallmeyer, J., 2021. Organic matter mineralization in modern and ancient ferruginous
938 sediments. *Nat. Commun.* 12, 2216. <https://doi.org/10.1038/s41467-021-22453-0>
- 939 Fry, B., 2021. 13C/12C fractionation by marine diatoms 13.
- 940 Fry, B., Jannasch, H.W., Molyneaux, S.J., Wirsén, C.O., Muramoto, J.A., King, S., 1991. Stable isotope
941 studies of the carbon, nitrogen and sulfur cycles in the Black Sea and the Cariaco Trench. *Deep Sea*
942 *Res. Part Oceanogr. Res. Pap.* 38, S1003–S1019. [https://doi.org/10.1016/S0198-0149\(10\)80021-4](https://doi.org/10.1016/S0198-0149(10)80021-4)
- 943 Fulton, J.M., Arthur, M.A., Thomas, B., Freeman, K.H., 2018. Pigment carbon and nitrogen isotopic
944 signatures in euxinic basins. *Geobiology* 16, 429–445. <https://doi.org/10.1111/gbi.12285>
- 945 Furian, S., Martins, E.R.C., Parizotto, T.M., Rezende-Filho, A.T., Victoria, R.L., Barbiero, L., 2013.
946 Chemical diversity and spatial variability in myriad lakes in Nhecolândia in the Pantanal wetlands of
947 Brazil. *Limnol. Oceanogr.* 58, 2249–2261. <https://doi.org/10.4319/lo.2013.58.6.2249>
- 948 Gérard, E., Ménez, B., Couradeau, E., Moreira, D., Benzerara, K., Tavera, R., López-García, P., 2013.
949 Specific carbonate–microbe interactions in the modern microbialites of Lake Alchichica (Mexico).
950 *ISME J.* 7, 1997–2009. <https://doi.org/10.1038/ismej.2013.81>
- 951 Gonzales-Partida, E., Barragan-R, R.M., Nieva-G, D., 1993. Analisis geoquímico-isotópico de las
952 especies carbonicas del fluido geotermico de Los Humeros, Puebla, México. *Geofis. Int.* 32, 299–309.
- 953 Gröger, J., Franke, J., Hamer, K., Schulz, H.D., 2009. Quantitative Recovery of Elemental Sulfur and
954 Improved Selectivity in a Chromium-Reducible Sulfur Distillation. *Geostand. Geoanalytical Res.* 33,
955 17–27. <https://doi.org/10.1111/j.1751-908X.2009.00922.x>
- 956 Gu, B., Schelske, C.L., Hodell, D.A., 2004. Extreme 13C enrichments in a shallow hypereutrophic lake:
957 Implications for carbon cycling. *Limnol. Oceanogr.* 49, 1152–1159.
958 <https://doi.org/10.4319/lo.2004.49.4.1152>
- 959 Hassan, K.M., 2014. Isotope geochemistry of Swan Lake Basin in the Nebraska Sandhills, USA: Large
960 13C enrichment in sediment-calcite records. *Geochemistry* 74, 681–690.
961 <https://doi.org/10.1016/j.chemer.2014.03.004>
- 962 Havig, J.R., Hamilton, T.L., McCormick, M., McClure, B., Sowers, T., Wegter, B., Kump, L.R., 2018.
963 Water column and sediment stable carbon isotope biogeochemistry of permanently redox-stratified
964 Fayetteville Green Lake, New York, U.S.A. *Limnol. Oceanogr.* 63, 570–587.
965 <https://doi.org/10.1002/lno.10649>
- 966 Havig, J.R., McCormick, M.L., Hamilton, T.L., Kump, L.R., 2015. The behavior of biologically important
967 trace elements across the oxic/euxinic transition of meromictic Fayetteville Green Lake, New York,
968 USA. *Geochim. Cosmochim. Acta* 165, 389–406. <https://doi.org/10.1016/j.gca.2015.06.024>

969 Hayes, J.M., Popp, B.N., Takigiku, R., Johnson, M.W., 1989. An isotopic study of biogeochemical
970 relationships between carbonates and organic carbon in the Greenhorn Formation. *Geochim.*
971 *Cosmochim. Acta* 53, 2961–2972. [https://doi.org/10.1016/0016-7037\(89\)90172-5](https://doi.org/10.1016/0016-7037(89)90172-5)

972 Hayes, J.M., Strauss, H., Kaufman, A.J., 1999. The abundance of ¹³C in marine organic matter and
973 isotopic fractionation in the global biogeochemical cycle of carbon during the past 800 Ma. *Chem.*
974 *Geol.* 161, 103–125. [https://doi.org/10.1016/S0009-2541\(99\)00083-2](https://doi.org/10.1016/S0009-2541(99)00083-2)

975 Henkel, J.V., Dellwig, O., Pollehne, F., Herlemann, D.P.R., Leipe, T., Schulz-Vogt, H.N., 2019. A
976 bacterial isolate from the Black Sea oxidizes sulfide with manganese(IV) oxide. *Proc. Natl. Acad. Sci.*
977 116, 12153–12155. <https://doi.org/10.1073/pnas.1906000116>

978 Hurley, S.J., Wing, B.A., Jasper, C.E., Hill, N.C., Cameron, J.C., 2021. Carbon isotope evidence for the
979 global physiology of Proterozoic cyanobacteria. *Sci. Adv.* 7, eabc8998.
980 <https://doi.org/10.1126/sciadv.abc8998>

981 Iniesto, M., Moreira, D., Benzerara, K., Muller, E., Bertolino, P., Tavera, R., López-García, P., 2021a.
982 Rapid formation of mature microbialites in Lake Alchichica, Mexico. *Environ. Microbiol. Rep.* 13, 600–
983 605. <https://doi.org/10.1111/1758-2229.12957>

984 Iniesto, M., Moreira, D., Benzerara, K., Reboul, G., Bertolino, P., Tavera, R., López-García, P., 2022.
985 Planktonic microbial communities from microbialite-bearing lakes sampled along a salinity-alkalinity
986 gradient. *Limnol. Oceanogr.* Ino.12233. <https://doi.org/10.1002/lno.12233>

987 Iniesto, M., Moreira, D., Reboul, G., Deschamps, P., Benzerara, K., Bertolino, P., Saghai, A., Tavera, R.,
988 López-García, P., 2021b. Core microbial communities of lacustrine microbialites sampled along an
989 alkalinity gradient. *Environ. Microbiol.* 23, 51–68. <https://doi.org/10.1111/1462-2920.15252>

990 Iñiguez, C., Capó-Bauçà, S., Niinemets, Ü., Stoll, H., Aguiló-Nicolau, P., Galmés, J., 2020. Evolutionary
991 trends in RuBisCO kinetics and their co-evolution with CO₂ concentrating mechanisms. *Plant J.* 101,
992 897–918. <https://doi.org/10.1111/tpj.14643>

993 Javoy, M., Pineau, F., Delorme, H., 1986. Carbon and nitrogen isotopes in the mantle. *Chem. Geol.,*
994 *Isotopes in Geology—Picciotto Volume* 57, 41–62. [https://doi.org/10.1016/0009-2541\(86\)90093-8](https://doi.org/10.1016/0009-2541(86)90093-8)

995 Jézéquel, D., Michard, G., Viollier, E., Agrinier, P., Albéric, P., Lopes, F., Abril, G., Bergonzini, L., 2016.
996 Carbon Cycle in a Meromictic Crater Lake: Lake Pavin, France, in: Sime-Ngando, T., Boivin, P.,
997 Chapron, E., Jezequel, D., Meybeck, M. (Eds.), *Lake Pavin: History, Geology, Biogeochemistry, and*
998 *Sedimentology of a Deep Meromictic Maar Lake.* Springer International Publishing, Cham, pp. 185–
999 203. https://doi.org/10.1007/978-3-319-39961-4_11

1000 Jiao, N., Herndl, G.J., Hansell, D.A., Benner, R., Kattner, G., Wilhelm, S.W., Kirchman, D.L., Weinbauer,
1001 M.G., Luo, T., Chen, F., Azam, F., 2010. Microbial production of recalcitrant dissolved organic matter:
1002 long-term carbon storage in the global ocean. *Nat. Rev. Microbiol.* 8, 593–599.
1003 <https://doi.org/10.1038/nrmicro2386>

1004 Jørgensen, B.B., 1982. Mineralization of organic matter in the sea bed—the role of sulphate
1005 reduction. *Nature* 296, 643–645. <https://doi.org/10.1038/296643a0>

1006 Karhu, J.A., Holland, H.D., 1996. Carbon isotopes and the rise of atmospheric oxygen. *Geology* 24,
1007 867. [https://doi.org/10.1130/0091-7613\(1996\)024<0867:CIATRO>2.3.CO;2](https://doi.org/10.1130/0091-7613(1996)024<0867:CIATRO>2.3.CO;2)

1008 Klawonn, I., Van den Wyngaert, S., Parada, A.E., Arandia-Gorostidi, N., Whitehouse, M.J., Grossart,
1009 H.-P., Dekas, A.E., 2021. Characterizing the “fungal shunt”: Parasitic fungi on diatoms affect carbon

1010 flow and bacterial communities in aquatic microbial food webs. *Proc. Natl. Acad. Sci.* 118,
1011 e2102225118. <https://doi.org/10.1073/pnas.2102225118>

1012 Knossow, N., Blonder, B., Eckert, W., Turchyn, A.V., Antler, G., Kamyshny, A., 2015. Annual sulfur
1013 cycle in a warm monomictic lake with sub-millimolar sulfate concentrations. *Geochem. Trans.* 16, 7.
1014 <https://doi.org/10.1186/s12932-015-0021-5>

1015 Krissansen-Totton, J., Buick, R., Catling, D.C., 2015. A statistical analysis of the carbon isotope record
1016 from the Archean to Phanerozoic and implications for the rise of oxygen. *Am. J. Sci.* 315, 275–316.
1017 <https://doi.org/10.2475/04.2015.01>

1018 Kuntz, L.B., Laakso, T.A., Schrag, D.P., Crowe, S.A., 2015. Modeling the carbon cycle in Lake Matano.
1019 *Geobiology* 13, 454–461. <https://doi.org/10.1111/gbi.12141>

1020 Lehmann, M.F., Bernasconi, S.M., Barbieri, A., McKenzie, J.A., 2002. Preservation of organic matter
1021 and alteration of its carbon and nitrogen isotope composition during simulated and in situ early
1022 sedimentary diagenesis. *Geochim. Cosmochim. Acta* 66, 3573–3584. [https://doi.org/10.1016/S0016-7037\(02\)00968-7](https://doi.org/10.1016/S0016-7037(02)00968-7)

1024 Lehmann, M.F., Bernasconi, S.M., McKenzie, J.A., Barbieri, A., Simona, M., Veronesi, M., 2004.
1025 Seasonal variation of the δC and δN of particulate and dissolved carbon and nitrogen in Lake Lugano:
1026 Constraints on biogeochemical cycling in a eutrophic lake. *Limnol. Oceanogr.* 49, 415–429.
1027 <https://doi.org/10.4319/lo.2004.49.2.0415>

1028 Lelli, M., Kretzschmar, T.G., Cabassi, J., Doveri, M., Sanchez-Avila, J.I., Gherardi, F., Magro, G., Norelli,
1029 F., 2021. Fluid geochemistry of the Los Humeros geothermal field (LHGF - Puebla, Mexico): New
1030 constraints for the conceptual model. *Geothermics* 90, 101983.
1031 <https://doi.org/10.1016/j.geothermics.2020.101983>

1032 Li, H.-C., Ku, T.-L., 1997. $\delta^{13}C$ – $\delta^{18}C$ covariance as a paleohydrological indicator for closed-basin
1033 lakes. *Palaeogeogr. Palaeoclimatol. Palaeoecol.* 133, 69–80. [https://doi.org/10.1016/S0031-0182\(96\)00153-8](https://doi.org/10.1016/S0031-0182(96)00153-8)

1035 Logan, G.A., Hayes, J.M., Hieshima, G.B., Summons, R.E., 1995. Terminal Proterozoic reorganization
1036 of biogeochemical cycles. *Nature* 376, 53–56. <https://doi.org/10.1038/376053a0>

1037 Lorenz, V., 1986. On the growth of maars and diatremes and its relevance to the formation of tuff
1038 rings. *Bull. Volcanol.* 48, 265–274. <https://doi.org/10.1007/BF01081755>

1039 Lugo, A., Alcocer, J., Sánchez, Ma. del R., Escobar, E., Macek, M., 2000. Temporal and spatial variation
1040 of bacterioplankton abundance in a tropical, warm-monomictic, saline lake: Alchichica, Puebla,
1041 Mexico. *SIL Proc. 1922-2010* 27, 2968–2971. <https://doi.org/10.1080/03680770.1998.11898217>

1042 Lugo, A., Alcocer, J., Sanchez, M.R., Escobar, E., 1993. Trophic status of tropical lakes indicated by
1043 littoral protozoan assemblages. *SIL Proc. 1922-2010* 25, 441–443.
1044 <https://doi.org/10.1080/03680770.1992.11900159>

1045 Lyons, T.W., Reinhard, C.T., Planavsky, N.J., 2014. The rise of oxygen in Earth's early ocean and
1046 atmosphere. *Nature* 506, 307–315. <https://doi.org/10.1038/nature13068>

1047 Macek, M., Medina, X.S., Picazo, A., Peřtová, D., Reyes, F.B., Hernández, J.R.M., Alcocer, J., Ibarra,
1048 M.M., Camacho, A., 2020. Spirostomum teres: A Long Term Study of an Anoxic-Hypolimnion
1049 Population Feeding upon Photosynthesizing Microorganisms. *Acta Protozool.* 59, 13–38.
1050 <https://doi.org/10.4467/16890027AP.20.002.12158>

- 1051 Mason, E., Edmonds, M., Turchyn, A.V., 2017. Remobilization of crustal carbon may dominate
1052 volcanic arc emissions. *Science* 357, 290–294. <https://doi.org/10.1126/science.aan5049>
- 1053 Mendonça, R., Müller, R.A., Clow, D., Verpoorter, C., Raymond, P., Tranvik, L.J., Sobek, S., 2017.
1054 Organic carbon burial in global lakes and reservoirs. *Nat. Commun.* 8, 1694.
1055 <https://doi.org/10.1038/s41467-017-01789-6>
- 1056 Mercedes-Martin, R., Ayora, C., Tritlla, J., Sánchez-Román, M., 2019. The hydrochemical evolution of
1057 alkaline volcanic lakes: a model to understand the South Atlantic Pre-salt mineral assemblages. *Earth-*
1058 *Sci. Rev.* 198, 102938. <https://doi.org/10.1016/j.earscirev.2019.102938>
- 1059 Milesi, V.P., Debure, M., Marty, N.C.M., Capano, M., Jézéquel, D., Steefel, C., Rouchon, V., Albéric, P.,
1060 Bard, E., Sarazin, G., Guyot, F., Virgone, A., Gaucher, É.C., Ader, M., 2020. Early Diagenesis of
1061 Lacustrine Carbonates in Volcanic Settings: The Role of Magmatic CO₂ (Lake Dziani Dzaha, Mayotte,
1062 Indian Ocean). *ACS Earth Space Chem.* 4, 363–378.
1063 <https://doi.org/10.1021/acsearthspacechem.9b00279>
- 1064 Mook, W.G., Bommerson, J.C., Staverman, W.H., 1974. Carbon isotope fractionation between
1065 dissolved bicarbonate and gaseous carbon dioxide. *Earth Planet. Sci. Lett.* 22, 169–176.
1066 [https://doi.org/10.1016/0012-821X\(74\)90078-8](https://doi.org/10.1016/0012-821X(74)90078-8)
- 1067 Mulholland, P.J., Elwood, J.W., 1982. The role of lake and reservoir sediments as sinks in the
1068 perturbed global carbon cycle. *Tellus* 34, 490–499. [https://doi.org/10.1111/j.2153-](https://doi.org/10.1111/j.2153-3490.1982.tb01837.x)
1069 [3490.1982.tb01837.x](https://doi.org/10.1111/j.2153-3490.1982.tb01837.x)
- 1070 O'Leary, M.H., 1988. Carbon Isotopes in Photosynthesis. *BioScience* 38, 328–336.
1071 <https://doi.org/10.2307/1310735>
- 1072 Pardue, J.W., Scalan, R.S., Van Baalen, C., Parker, P.L., 1976. Maximum carbon isotope fractionation
1073 in photosynthesis by blue-green algae and a green alga. *Geochim. Cosmochim. Acta* 40, 309–312.
1074 [https://doi.org/10.1016/0016-7037\(76\)90208-8](https://doi.org/10.1016/0016-7037(76)90208-8)
- 1075 Peiffer, L., Carrasco-Núñez, G., Mazot, A., Villanueva-Estrada, R.E., Inguaggiato, C., Bernard Romero,
1076 R., Rocha Miller, R., Hernández Rojas, J., 2018. Soil degassing at the Los Humeros geothermal field
1077 (Mexico). *J. Volcanol. Geotherm. Res.* 356, 163–174.
1078 <https://doi.org/10.1016/j.jvolgeores.2018.03.001>
- 1079 Petrash, D.A., Steenbergen, I.M., Valero, A., Meador, T.B., Pačes, T., Thomazo, C., 2022. Aqueous
1080 system-level processes and prokaryote assemblages in the ferruginous and sulfate-rich bottom
1081 waters of a post-mining lake. *Biogeosciences* 19, 1723–1751. [https://doi.org/10.5194/bg-19-1723-](https://doi.org/10.5194/bg-19-1723-2022)
1082 [2022](https://doi.org/10.5194/bg-19-1723-2022)
- 1083 Pimenov, N.V., Lunina, O.N., Prusakova, T.S., Rusanov, I.I., Ivanov, M.V., 2008. Biological fractionation
1084 of stable carbon isotopes at the aerobic/anaerobic water interface of meromictic water bodies.
1085 *Microbiology* 77, 751–759. <https://doi.org/10.1134/S0026261708060131>
- 1086 Posth, N.R., Bristow, L.A., Cox, R.P., Habicht, K.S., Danza, F., Tonolla, M., Frigaard, N. -U., Canfield,
1087 D.E., 2017. Carbon isotope fractionation by anoxygenic phototrophic bacteria in euxinic Lake
1088 Cadagno. *Geobiology* 15, 798–816. <https://doi.org/10.1111/gbi.12254>
- 1089 Rendon-Lopez, M.J., 2008. Limnología física del lago crater los Espinos, Municipio de Jiménez
1090 Michoacan.

- 1091 Ridgwell, A., Arndt, S., 2015. Chapter 1 - Why Dissolved Organics Matter: DOC in Ancient Oceans and
1092 Past Climate Change, in: Hansell, D.A., Carlson, C.A. (Eds.), Biogeochemistry of Marine Dissolved
1093 Organic Matter (Second Edition). Academic Press, Boston, pp. 1–20. <https://doi.org/10.1016/B978-0-12-405940-5.00001-7>
1094
- 1095 Sackett, W.M., Eckelmann, W.R., Bender, M.L., Bé, A.W.H., 1965. Temperature Dependence of
1096 Carbon Isotope Composition in Marine Plankton and Sediments. *Science* 148, 235–237.
1097 <https://doi.org/10.1126/science.148.3667.235>
- 1098 Saghaï, A., Zivanovic, Y., Moreira, D., Benzerara, K., Bertolino, P., Ragon, M., Tavera, R., López-
1099 Archilla, A.I., López-García, P., 2016. Comparative metagenomics unveils functions and genome
1100 features of microbialite-associated communities along a depth gradient: Comparative metagenomics
1101 of microbialites from Lake Alchichica. *Environ. Microbiol.* 18, 4990–5004.
1102 <https://doi.org/10.1111/1462-2920.13456>
- 1103 Saini, J.S., Hassler, C., Cable, R., Fourquez, M., Danza, F., Roman, S., Tonolla, M., Storelli, N., Jacquet,
1104 S., Zdobnov, E.M., Duhaime, M.B., 2021. Microbial loop of a Proterozoic ocean analogue (preprint).
1105 *Microbiology*. <https://doi.org/10.1101/2021.08.17.456685>
- 1106 Satkoski, A.M., Beukes, N.J., Li, W., Beard, B.L., Johnson, C.M., 2015. A redox-stratified ocean 3.2
1107 billion years ago. *Earth Planet. Sci. Lett.* 430, 43–53. <https://doi.org/10.1016/j.epsl.2015.08.007>
- 1108 Schidlowski, M., 2001. Carbon isotopes as biogeochemical recorders of life over 3.8 Ga of Earth
1109 history: evolution of a concept. *Precambrian Res.* 106, 117–134. [https://doi.org/10.1016/S0301-9268\(00\)00128-5](https://doi.org/10.1016/S0301-9268(00)00128-5)
1110
- 1111 Schiff, S.L., Tsuji, J.M., Wu, L., Venkiteswaran, J.J., Molot, L.A., Elgood, R.J., Paterson, M.J., Neufeld,
1112 J.D., 2017. Millions of Boreal Shield Lakes can be used to Probe Archaean Ocean Biogeochemistry.
1113 *Sci. Rep.* 7, 46708. <https://doi.org/10.1038/srep46708>
- 1114 Siebe, C., Guilbaud, M.-N., Salinas, S., Chédeville-Monzo, C., 2012. Eruption of Alberca de los Espinos
1115 tuff cone causes transgression of Zacapu lake ca. 25,000 yr BP in Michoacán, México. Presented at
1116 the IAS 4IMC Conference, Auckland, New Zeland, pp. 74–75.
- 1117 Siebe, C., Guilbaud, M.-N., Salinas, S., Kshirsagar, P., Chevrel, M.O., Jiménez, A.H., Godínez, L., 2014.
1118 Monogenetic volcanism of the Michoacán-Guanajuato Volcanic Field: Maar craters of the Zacapu
1119 basin and domes, shields, and scoria cones of the Tarascan highlands (Paracho-Paricutin region).
1120 Presented at the Pre-meeting field guide for the 5th international Maar Conference, Querétaro,
1121 México, pp. 1–37.
- 1122 Sigala, I., Caballero, M., Correa-Metrio, A., Lozano-García, S., Vázquez, G., Pérez, L., Zawisza, E., 2017.
1123 Basic limnology of 30 continental waterbodies of the Transmexican Volcanic Belt across climatic and
1124 environmental gradients. *Bol. Soc. Geológica Mex.* 69, 313–370.
1125 <https://doi.org/10.18268/BSGM2017v69n2a3>
- 1126 Silva Aguilera, R.A., 2019. Analisis del descenso del nivel de agua del lago Alchichica, Puebla, México
1127 120.
- 1128 Sirevag, R., Buchanan, B.B., Berry, J.A., Troughton, J.H., 1977. Mechanisms of CO₂ Fixation in Bacterial
1129 Photosynthesis Studied by the Carbon Isotope Fractionation Technique. *Arch Microbiol* 112, 4.

1130 Sobek, S., Durisch-Kaiser, E., Zurbrügg, R., Wongfun, N., Wessels, M., Pasche, N., Wehrli, B., 2009.
1131 Organic carbon burial efficiency in lake sediments controlled by oxygen exposure time and sediment
1132 source. *Limnol. Oceanogr.* 54, 2243–2254. <https://doi.org/10.4319/lo.2009.54.6.2243>

1133 Soetaert, K., Hofmann, A.F., Middelburg, J.J., Meysman, F.J.R., Greenwood, J., 2007. The effect of
1134 biogeochemical processes on pH. *Mar. Chem.* 105, 30–51.
1135 <https://doi.org/10.1016/j.marchem.2006.12.012>

1136 Talbot, M.R., 1990. A review of the palaeohydrological interpretation of carbon and oxygen isotopic
1137 ratios in primary lacustrine carbonates. *Chem. Geol. Isot. Geosci. Sect.* 80, 261–279.
1138 [https://doi.org/10.1016/0168-9622\(90\)90009-2](https://doi.org/10.1016/0168-9622(90)90009-2)

1139 Thomas, P.J., Boller, A.J., Satagopan, S., Tabita, F.R., Cavanaugh, C.M., Scott, K.M., 2019. Isotope
1140 discrimination by form IC RubisCO from *Ralstonia eutropha* and *Rhodobacter sphaeroides*,
1141 metabolically versatile members of ‘*Proteobacteria*’ from aquatic and soil habitats. *Environ.*
1142 *Microbiol.* 21, 72–80. <https://doi.org/10.1111/1462-2920.14423>

1143 Ussiri, D.A.N., Lal, R., 2017. Carbon Sequestration for Climate Change Mitigation and Adaptation.
1144 Springer International Publishing, Cham. <https://doi.org/10.1007/978-3-319-53845-7>

1145 Van Mooy, B.A.S., Keil, R.G., Devol, A.H., 2002. Impact of suboxia on sinking particulate organic
1146 carbon: Enhanced carbon flux and preferential degradation of amino acids via denitrification.
1147 *Geochim. Cosmochim. Acta* 66, 457–465. [https://doi.org/10.1016/S0016-7037\(01\)00787-6](https://doi.org/10.1016/S0016-7037(01)00787-6)

1148 Vilaclara, G., Chávez, M., Lugo, A., González, H., Gaytán, M., 1993. Comparative description of crater-
1149 lakes basic chemistry in Puebla State, Mexico. *SIL Proc.* 1922-2010 25, 435–440.
1150 <https://doi.org/10.1080/03680770.1992.11900158>

1151 Vliet, D.M., Meijnenfeldt, F.A.B., Dutilh, B.E., Villanueva, L., Sinninghe Damsté, J.S., Stams, A.J.M.,
1152 Sánchez-Andrea, I., 2021. The bacterial sulfur cycle in expanding dysoxic and euxinic marine waters.
1153 *Environ. Microbiol.* 23, 2834–2857. <https://doi.org/10.1111/1462-2920.15265>

1154 Vuillemin, A., Friese, A., Alawi, M., Henny, C., Nomosatryo, S., Wagner, D., Crowe, S.A., Kallmeyer, J.,
1155 2016. Geomicrobiological Features of Ferruginous Sediments from Lake Towuti, Indonesia. *Front.*
1156 *Microbiol.* 7. <https://doi.org/10.3389/fmicb.2016.01007>

1157 Wang, S., Yeager, K.M., Lu, W., 2016. Carbon isotope fractionation in phytoplankton as a potential
1158 proxy for pH rather than for [CO₂(aq)]: Observations from a carbonate lake. *Limnol. Oceanogr.* 61,
1159 1259–1270. <https://doi.org/10.1002/lno.10289>

1160 Werne, J.P., Hollander, D.J., 2004. Balancing supply and demand: controls on carbon isotope
1161 fractionation in the Cariaco Basin (Venezuela) Younger Dryas to present. *Mar. Chem.* 92, 275–293.
1162 <https://doi.org/10.1016/j.marchem.2004.06.031>

1163 Whiticar, M.J., Faber, E., Schoell, M., 1986. Biogenic methane formation in marine and freshwater
1164 environments: CO₂ reduction vs. acetate fermentation—Isotope evidence. *Geochim. Cosmochim.*
1165 *Acta* 50, 693–709. [https://doi.org/10.1016/0016-7037\(86\)90346-7](https://doi.org/10.1016/0016-7037(86)90346-7)

1166 Williams, P.M., Gordon, L.I., 1970. Carbon-13: carbon-12 ratios in dissolved and particulate organic
1167 matter in the sea. *Deep Sea Res. Oceanogr. Abstr.* 17, 19–27. [https://doi.org/10.1016/0011-7471\(70\)90085-9](https://doi.org/10.1016/0011-7471(70)90085-9)

- 1169 Wittkop, C., Teranes, J., Lubenow, B., Dean, W.E., 2014. Carbon- and oxygen-stable isotopic
1170 signatures of methanogenesis, temperature, and water column stratification in Holocene siderite
1171 varves. *Chem. Geol.* 389, 153–166. <https://doi.org/10.1016/j.chemgeo.2014.09.016>
- 1172 Zeyen, N., Benzerara, K., Beyssac, O., Daval, D., Muller, E., Thomazo, C., Tavera, R., López-García, P.,
1173 Moreira, D., Duprat, E., 2021. Integrative analysis of the mineralogical and chemical composition of
1174 modern microbialites from ten Mexican lakes: What do we learn about their formation? *Geochim.
1175 Cosmochim. Acta* 305, 148–184. <https://doi.org/10.1016/j.gca.2021.04.030>
- 1176 Zohary, T., Erez, J., Gophen, M., Berman-Frank, I., Stiller, M., 1994. Seasonality of stable carbon
1177 isotopes within the pelagic food web of Lake Kinneret. *Limnol. Oceanogr.* 39, 1030–1043.
1178 <https://doi.org/10.4319/lo.1994.39.5.1030>
- 1179 Zyakun, A.M., Lunina, O.N., Prusakova, T.S., Pimenov, N.V., Ivanov, M.V., 2009. Fractionation of
1180 stable carbon isotopes by photoautotrophically growing anoxygenic purple and green sulfur bacteria.
1181 *Microbiology* 78, 757–768. <https://doi.org/10.1134/S0026261709060137>
- 1182